ON THE OXIDATIVE HALF-REACTION OF *PLASMODIUM FALCIPARUM* DIHYDROOROTATE DEHYDROGENASE

APPROVED BY SUPERVISORY COMMITTEE

Margaret A. Phillips, Ph.D.

Joseph P. Albanesi, Ph.D.

Richard J. Auchus, M.D., Ph.D.

Alfred G. Gilman, M.D., Ph.D.

DEDICATION

For my wife, Camille.

ON THE OXIDATIVE HALF-REACTION OF *PLASMODIUM FALCIPARUM* DIHYDROOROTATE DEHYDROGENASE

by

NICHOLAS ANTHONY MALMQUIST

DISSERTATION

Presented to the Faculty of the Graduate School of Biomedical Sciences

The University of Texas Southwestern Medical Center at Dallas

In Partial Fulfillment of the Requirements

For the Degree of

DOCTOR OF PHILOSOPHY

The University of Texas Southwestern Medical Center at Dallas

Dallas, Texas

September, 2007

ON THE OXIDATIVE HALF-REACTION OF *PLASMODIUM FALCIPARUM* DIHYDROOROTATE DEHYDROGENASE

Publication No. _____

Nicholas Anthony Malmquist, Ph.D.

The University of Texas Southwestern Medical Center at Dallas, 2007

Supervising Professor: Margaret A. Phillips, Ph.D.

Plasmodium falciparum is the parasite responsible for an estimated 500 million malaria cases per year, which result in 1-2 million annual deaths. Current antimalarial chemotherapies are met with the tremendous ability of the parasite to develop resistance, underscoring the need for newer, more potent antimalarial drugs. Survival of the malaria parasite is dependent upon *de novo* biosynthesis of pyrimidines, as the organism is deficient in pyrimidine salvage. Dihydroorotate dehydrogenase (DHODH) is the flavoenzyme which catalyzes the fourth step in

this pathway. The studies presented here describe the oxidative half-reaction of *Pf* DHODH where the enzyme, containing reduced falvin mononucleotide (FMN), is re-oxidized by terminal electron acceptors. The lipophilic co-substrate ubiquinone (CoQ) is shown to partition into detergent micelles in a hydrophobic chain length-dependent manner. Additionally, the enzyme is shown to associate with liposomes, which is likely mediated by its hydrophobic N-terminal domain. This arrangement reflects the physiological location of CoQ co-substrates within, and the attachment of the enzyme to, the inner mitochondrial membrane. Catalysis of CoQ analogues which partition into detergent micelles fit well to a surface dilution kinetic model, while catalysis of a CoQ analogue which remains in solution is well described by a solution steady-state kinetic model. These results suggest that the enzyme can perform catalysis of hydrophobic CoQ co-substrates at the surface-solution interface. Steady-state kinetic analysis of the complete *Pf* DHODH reaction cycle revealed only a modest alteration in the K_M^{app} for CoQ analogues upon mutation of several CoQ binding site residues to alanine, but displayed a more substantial effect on the catalytic rate upon mutation of a subset of residues. Pre-steady-state kinetic analysis showed both the dihydroorotate (DHO)-dependent half-reaction and the CoQ-dependent half-reaction to be faster than the observed steady-state rate. The A77 1726 binding-site mutations had no effect on the rate of the reductive half-reaction, but several reduced the rate of the CoQ-dependent flavin oxidation step without significantly altering the K_d for

CoQ. Inhibitors which bind in the proposed CoQ site block the CoQ-dependent oxidative half-reaction but do not inhibit the DHO-dependent reductive half-reaction. These results clearly distinguish the two co-substrate binding sites for DHO and CoQ and identify residues involved in electron transfer to physiologically relevant terminal electron acceptor substrates at a distant site.

TABLE OF CONTENTS

PRIOR PUBLICATIONS

Work cited in this dissertation:

1. **Malmquist NA**, Gujjar R, Rathod PK, Phillips MA. (2007) "Analysis of flavin oxidation and electron transfer inhibition in *Plasmodium falciparum* dihydroorotate dehydrogenase." Biochemistry *submitted*.

2. **Malmquist NA**, Baldwin J, Phillips MA. (2007) "Detergent-dependent kinetics of *Plasmodium falciparum* dihydroorotate dehydrogenase." J Biol Chem **282**(17):12678-86.

3. Baldwin J, Michnoff CH, **Malmquist NA**, White J, Roth MG, Rathod PK, Phillips MA. (2005) "High-throughput screening for potent and selective inhibitors of *Plasmodium falciparum* dihydroorotate dehydrogenase." J Biol Chem **280**(23):21847-53.

4. Baldwin J, Farajallah AM, **Malmquist NA**, Rathod PK, Phillips MA. (2002) "Malarial dihydroorotate dehydrogenase. Substrate and inhibitor specificity." J Biol Chem **277**(44): 41827-34.

Other work:

5. Gruszynski AE, van Deursen FJ, Albareda MC, Best A, Chaudhary K, Cliffe LJ, Del Rio L, Dunn JD, Ellis L, Evans KJ, Figueiredo JM, **Malmquist NA**, Omosun Y, Palenchar JB, Prickett S, Punkosdy GA, van Dooren G, Wang Q, Menon AK, Matthews KR, Bangs JD. (2006) "Regulation of surface coat exchange by differentiating African trypanosomes." Mol Biochem Parasitol **147**(2):211-223.

6. Tichenor SD, **Malmquist NA**, Buxton IL. (2003) "Dissociation of cGMP accumulation and relaxation in myometrial smooth muscle: effects of S-nitroso-N-acetylpenicillamine and 3-morpholinosyndonimine." Cell Signal **15**(8):763-72.

7. Buxton ILO, Kaiser RA, **Malmquist NA**, Tichenor S. (2001) "NO-induced relaxation of labouring and non-labouring human myometrium is not mediated by cyclic GMP." Br J Pharmacol **134**(1): 206-14.

8. Tichenor S, **Malmquist NA**, Buxton ILO. (2001) "Actions of S-nitroso N-acetyl penicillamine and 3-morpholinosydonimine may involve disparate

signaling pathways in myometrial smooth muscle." Proc West Pharmacol Soc **44**: 53-6.

9. **Malmquist NA**, Anzinger JJ, Hirzel D, Buxton ILO. (2001) "Ellagic acid inhibits nucleoside diphosphate kinase-B activity." Proc West Pharmacol Soc **44**: 57-9.

10. Anzinger J, **Malmquist NA**, Gould J, Buxton ILO. (2001) "Secretion of a nucleoside diphosphate kinase (Nm23-H2) by cells from human breast, colon, pancreas and lung tumors." Proc West Pharmacol Soc **44**: 61-3.

LIST OF EQUATIONS

LIST OF SCHEMES

LIST OF TABLES

LIST OF FIGURES

LIST OF DEFINITIONS

A77 1726 - (Z)-2-cyano-3-hydroxy-N-(4-(trifluoromethyl)phenyl)but-2-enamide

C_8E_5 – pentaethylene glycol mono octyl ether

CD – circular dichroism

CMC – critical micelle concentration

CoQ – ubiquinone

CoQ_n – ubiquinone-n (n isoprene units)

CoQ_D – decylubiquinone

DCIP – 2,6-dichloroindophenol

DCPMNB – N-(3,5-dichloro-phenyl)-2-methyl-3-nitro-benzamidine

FAD – reduced flavin adenine dinucleotide

FMN – flavin mononucleotide

IPTG – isopropyl-beta-D-thiogalactopyranoside

ITC – isothermal titration calorimetry

L-DHO – dihydroorotate

NAD^+ – reduced nicotinamide adenine dinucleotide

PC – phosphatidylcholine

PE – phsophatidylethanolamine

Pf DHODH – *Plasmodium falciparum* dihydroorotate dehydrogenase

SEM – standard error of the mean

CHAPTER ONE
Background

MALARIA

Disease Aspects

The World Heath Organization estimates that 40% of the world's population is at risk of malaria. Of those 2.5 billion people, 500 million contract the disease every year, ultimately resulting in one to two million annual deaths. The at-risk population is primarily in the world's poorest countries located in the tropics, mostly sub-Saharan Africa but also in Latin America, Asia, and the Middle East. The majority of the malaria burden is felt in the vulnerable populations of children under five years of age and pregnant women. An estimated one in five of all childhood deaths in Africa are due to malaria and an African child has, on average, one to five episodes of malaria fever per year. Pregnant women are not only at risk for the complications of malaria felt in the general adult population but may also experience spontaneous abortion or premature delivery. These events account for one third of preventable low birth weight babies and are a factor in the deaths of an estimated 10,000 pregnant women and 200,000 infants annually in Africa.

Early symptoms of the disease include fever, chills, headache, and vomiting, which makes malaria particularly hard to distinguish from other typical diseases and hampers early diagnosis. As the disease progresses, metabolic

acidosis, severe anemia, and/or cerebral malaria may occur and ultimately prove fatal. Numerous host factors affect the clinical outcome of any particular malaria infection [1]. These include the possession of sickle cell or thalassemia blood disorders, age of the individual, pregnancy state, or partial immunity due to previous infection, the last of which remains poorly understood.

Parasites

Malaria is caused by parasitic protozoa of the *Plasmodium* genus, which are transmitted from host to host by *Anopheles* mosquitoes. The four *Plasmodium* species which cause disease in human are *P. falciparum*, *P. vivax*, *P. malariae*, and *P. ovale*, although *P. falciparum* is responsible for 80% of infections and 90% of malaria deaths [2]. Other *Plasmodium* species are known to specifically infect a variety of vertebrates including other mammals, birds, and reptiles. *Plasmodium* belong to the phylum apicomplexa, which includes other parasites including *Toxoplasma* and *Eimeria*. The name arises from the apical organization of these unicellular organisms, all of which possess various secretory organelles at their apical end which are implicated in host cell invasion. In addition, obligate parasite apicomplexan organisms contain a relic plastid, termed the "apicoplast," which originated from the engulfment of a red alga [3]. This plastid is of prokaryotic origin, and as such, contains genes involved in several metabolic pathways, including fatty acid and aromatic acid biosynthesis, which are distinct from or absent in the host [4].

Plasmodium parasites complete a complex life-cycle between the host and vector. Beginning at host infection, invasive sporozoites are injected into the host from the mosquito salivary glands. These sporozoites eventually reach the bloodstream and travel to the liver, where they invade hepatocytes and undergo a round of asexual replication that produces thousands of merozoites. Merozoites are shed from infected liver cells into the bloodstream, where they almost immediately invade erythrocytes (within one to two minutes). Each merozoite undergoes another round of asexual replication within the erythrocyte to produce roughly twenty new merozoites. The erythrocyte eventually bursts and the erythrocytic cycle of malaria continues. It is this erythrocytic cycle that corresponds to the cycle of fever and chills associated with malaria infection. Intraerythrocytic stage parasites also produce gametocytes, which may be picked up by a mosquito during a blood meal. These gametocytes are then induced to develop into gametes in the mosquito gut, and the resulting gametes sexually reproduce to form an ookinete. Ookinetes migrate through the mosquito gut epithelial cells to develop into oocysts, which undergo asexual replication to produce multiple sporozoites. Sporozoites traverse to the mosquito salivary glands, where they are ready to infect another host.

Intraerythrocytic development of *Plasmodium* parasites requires the full activity of several biochemical pathways to support the considerable amplification of the parasite genome and provide materials for the production of approximately

20 merozoites from the single merozoite which initially invaded the cell. During invasion of an erythrocyte, the parasite forms a parasitophorous vacuole which surrounds the parasite within the host cell and is permeable to many metabolites. The primary source of material for both energy production and cellular growth and division exists as host-cell hemoglobin. An arsenal of parasite-specific proteases exists to facilitate the degradation of hemoglobin, which occurs in a specialized parasite organelle called the food vacuole. A consequence of utilizing hemoglobin as a source of amino acids for growth and energy is the release of free heme, which is ultimately toxic. *Plasmodium* parasites have developed the means to polymerize free heme into crystalline hemozoin, the characteristic malaria pigment seen in the microscope, though the mechanism of the heme polymerization by the parasite is not fully understood. To provide the nucleotides necessary for the massive amplification of the parasite genome, *Plasmodium* parasites rely upon salvage pathways to obtain purines, for which they are deficient in *de novo* biosynthesis, and rely upon the *de novo* biosynthesis of pyrimidines, for which they are deficient in salvage.

Each host stage of the parasite life-cycle is potentially a target of antimalarial drugs and/or vaccines. The initially invasive sporozoite stage is both short lived and unpredictable, and therefore most promising as a vaccine target. However, the development of an effective vaccine against this or any other stage of the parasite life-cycle has proven unsuccessful thus far. Liver stage parasites

are only resident temporarily and are virtually undetectable and protected from the host immune system, suggesting this stage would be most difficult to target with any therapy. The most prevalent stage, and the one responsible for the devastating effects of the disease, is the intraerythrocytic stage. This stage presents the most viable option for chemotherapeutic intervention. The final host stage of the parasite life-cycle, development of the sexual stage gametocytes, is a potential target of "altruistic" vaccines, which would not cure disease in the patient, but would prevent transmission to additional hosts with the goal of breaking the host life-cycle.

Chemotherapy

History

The discovery of natural substances and subsequent development of synthetic compounds to target malaria parasites has a long and rich history and has been reviewed extensively [5-7]. Long before *Plasmodium* parasites were identified and linked to the disease in the 1880's by Alphonse Laveran, Ronald Ross, Battista Grasi, and others, a number of treatments for the periodic fever now known to be caused by malaria were described. Two of note are the Western treatment quinine and the Eastern treatment qinghao. Quinine, extracted from the bark of the South American chinchona tree and used in herbal remedies there, was introduced into Europe in the early 17th century. Quinine was eventually isolated from the bark in the 1820's and, as such, malaria is one the first diseases to be

treated by a pure chemical compound. Qinghao, or sweet wormwood, was used in China to treat fevers as early as the late 16th century. A government-sponsored systematic examination of herbal remedies in China in the late 1960's proved qinghao to be effective against malaria and less than a decade later the active component was isolated. The active component of qinghao and its derivatives are now used in Southeast Asia as antimalarial treatments and form the basis of an entire class of newly developed anti-malarial compounds.

Synthetic organic chemistry and the search for new antimalarial compounds augmented each other in the mid- to late-19th century. The first attempt to synthesize quinine in 1856 by the English chemist William Henry Perkins was unsuccessful. However, in the process the first synthetic textile dye, "mauve," was discovered. This spurred an entire commercial dye industry, the products of which were also useful in medical applications as stains for cells, microorganisms, and pathogens. The German scientist Paul Ehrlich observed *Plasmodium* parasites were particularly well stained by the dye methylene blue, and, in 1891, used the dye to cure malaria in two patients. This was the first time a synthetic drug was used to cure a disease in humans. Since then, European colonialism and two world wars have motivated the development of increasingly efficacious antimalarials.

Current Antimalarials & Modes of Action

Chloroquine (Figure 1-1) is the first successful quinoline antimalarial, based upon quinine, which enjoyed widespread usage. Cholorquine was developed during World War II and was a key component, along with the insecticide DDT, of the WHO Global Eradication Program of the 1950's and 1960's. This antimalarial was so effective that it was added to table salt in South America in a prophylaxis effort. Unfortunately, the extensive use of chloroquine quickly resulted in the development of chloroquine resistance, which presently exists throughout the world where malaria is endemic. In the few areas where chloroquine resistance does not exist, the compound remains highly effective when used judiciously. Several derivative quinoline antimalarial compounds have been developed and are currently in use. These include amodiaquine, mefloquine, halofantrane, and lumefantrine (Figure 1-1). Quinoline antimalarials concentrate in the food vacuole of the intraerythrocytic parasite. There, they appear to obstruct the polymerization of heme into crystalline hemozoin. This allows toxic free heme to accumulate, which may promote the disruption of cell membranes and produce destructive free radicals within the parasite. This non-host target has resulted in the relatively slow development of resistance to quinoline antimalarials. Indeed, the genetic markers associated with parasite resistance to quinoline compounds are found in food vacuole membrane transporters and not metabolic or catabolic enzymes [8, 9].

Derivatives of artemisinin (Figure 1-2), the active ingredient of qinghao, have also been successfully developed as antimalarial compounds. These compounds, including artemether, arteether, and artesunate, are metabolized to dihydroartemesinin, which is the active form in the body. These compounds contain an endo-peroxide bridge which was thought to undergo cleavage in the food vacuole, possibly through an interaction with heme-iron, to produce destructive free radicals. More recent evidence suggests the target of aretimisinin is a calcium-dependent ATPase located on the parasite endoplasmic reticulum [10], though that may not be the only cellular target of this free-radical producing compound. Artemisinin remains a potent antimalarial and is in current use in combination with other drugs in an effort to avoid the development of resistance.

The site of action of the antimalarial hydroxynaphthoquinone atovaquone (Figure 1-2) is the mitochondrial electron transport chain. This was discovered due to the unfortunately rapid onset of resistance to this compound brought about by a single point mutation in cytochrome *c* reductase [11]. Atovaquone is very successful when used in combination with proguanil, though cost and the potential for resistance limit the use of this drug combination to prophylaxis to first-world travelers who can afford it.

The antifolate compounds pyrimethamine and sulfadoxine (Figure 1-2) were the first antimalarial drugs to be developed with knowledge of cell biology in combination with synthetic medicinal chemistry. These compounds act to

inhibit the production of reduced folate cofactors, which are required for nucleotide biosynthesis. Pyrimethamine inhibits dihydrofolate reductase and sulfadoxine is an inhibitor of dihydropteroate synthase. As such, the combination therapy acts synergistically, thereby reducing the potential for resistance. However, the extensive use of this combination therapy has resulted in the development of resistance over time.

Plasmodium parasites are also sensitive to several common antibiotics, including tetracycline, doxycycline, and clindamycin [6]. The mode of action of antibiotics is thought to be the inhibition of metabolism in the apicoplast, as those metabolic pathways are essentially prokaryotic. The use of these drugs is limited to combination therapy in adults, as some antibiotics are contraindicated for use in children.

All of the aforementioned antimalarials have produced some degree of resistance in *Plasmodium* parasites, either in the field or in the laboratory. Many of the parent compounds have formed the basis for the production of derivatives with increasing efficacy, but the gains from these synthetic efforts are diminishing as the drug targets accumulate mutations which abrogate the effectiveness of any particular antimalarial and its derivatives. More prudent use of these compounds through combination therapy, where two or more drugs are used together, has helped to allay the development of resistance to some degree. However, drug

resistance to the available antimalarials is increasing, and this prompts the discovery of new drug targets to combat the malaria parasite.

Potential Small Molecule Drug Targets

Potential antimalarial drug targets arise due to a difference in drug affinity for the same target in the parasite versus the host cell, differences in the physiology between the parasite and the host, or unique targets in the parasite. Some drug targets possess two or all three of these characteristics, and numerous candidates exist and are being explored for the future exploitation by chemical therapeutics.

Candidate targets based on host-parasite differences at the molecular level include enzymes involved in glycolysis and membrane transporters responsible for the uptake of nutrients. The malaria parasite does not appear to possess a functional electron transport chain, and, as such, relies exclusively on glycolysis for the production of energy. Additionally, the rapid growth and replication of the parasite requires the efficient uptake of nutrients from the external milieu. Some of the potential target proteins in these parasite processes exist in both the host and parasite, and it is specific molecular variations in the target proteins that are being exploited to generate specificity. One example of this class is *Plasmodium* glycolytic enzyme lactate dehydrogenase, which exhibits differential inhibitor specificity between the parasite and human enzyme [12].

Differences in parasite and host-cell physiology highlight inhibitors of purine salvage as potential antimalarial drug targets, as the parasite is deficient in *de novo* biosynthesis and relies upon salvage of these molecules [13]. Conversely, the *de novo* pyrimidine biosynthesis pathway is a potential antimalarial drug target, as the parasite is deficient in salvage of pre-formed pyrimidine bases [13]. *Plasmodium* dihydroorotate dehydrogenase is a potential target due to its key role in *de novo* pyrimidine biosynthesis.

Novel processes in *Plasmodium*, such as hemoglobin degradation, heme polymerization, and pathways present in the apicoplast (plastid DNA replication and transcription, type II fatty acid biosynthesis, and non-mevalonate isoprenyl biosynthesis) offer high potential as specific parasite drug targets due to their exclusive utilization in the parasite. The identification protease inhibitors aimed toward hemoglobin degradation has yielded few potential antimalarials to date, and compounds directed toward the inhibiting heme polymerization are primarily based on derivatives of chloroquine. However, compounds which target the apicoplast type II fatty acid biosynthesis [14] and isoprenoid biosynthesis pathways [15] have proven promising.

DIHYDROOROTATE DEHYDROGENASE

Pyrimidine Biosynthesis

The pyrimidines bases uracil, cytosine, and thymine are the building blocks of DNA and RNA; they form the thymidine and cytidine deoxynucleotides

in DNA and the uridine and cytidine nucleotides in RNA. Pyrimidine derivatives are also used to form activated intermediates in a number of biosynthetic pathways: UDP-glucose is a precursor of glycogen and CDP-diacylglycerol is a precursor of phosphoglycerides. As such, a readily available pool of pyrimidines is necessary for the proper growth and division of all unicellular organisms and all dividing cells of multicellular organisms.

In contrast to purine biosynthesis, the pyrimidine base is synthesized first before being linked to the ribose sugar to form pyrimidine nucleosides (Figure 1-3). Pyrimidine biosynthesis begins with the formation of carbamoyl phosphate from glutamine and bicarbonate by carbamoyl phosphate synthetase. The committed step of pyrimidine biosynthesis occurs as carbamoyl phosphate is joined to aspartate by aspartate transcarbamoylase to form N-carbamoylaspartate. The pyrimidine ring is formed as N-carbamoylaspartate is cyclized with the loss of water by dihydroorotase to form dihydroorotate. Dihydroorotate is oxidized to orotate by dihydroorotate dehydrogenase. The ribose ring is then added to orotate as activated phosphoribose pyrophosphate by orotate phosphoribosyl transferase to form orotidylate. Orotidylate decarboxylase converts orotidylate to uridylate (also known as uridine monophosphate, UMP), the first major pyrimidine nucleotide.

Five pyrimidine biosynthesis enzymes are grouped into two complexes in higher eukaryotes: carbamoyl phosphate synthetase, aspartate transcarbamoylase,

and dihydroorotase form the so-called CAD complex while orotate phosphoribosyl transferase and orotidylate dexarboxylase associate to form a bifunctional complex. Dihydroorotate dehydrogenase is the only isolated enzyme in these organisms. It has been observed in *Plasmodium falciparum* that the last two enzymes of pyrimidine biosynthesis do not associate as they do in higher eukaryotes [16]. In prokaryotes, the six pyrimidine biosynthesis enzymes are not associated.

Enzyme Structure

The dihydroorotate dehydrogenase (DHODH) enzymes are flavin-containing α/β barrel proteins which catalyze the conversion of dihydroorotate (DHO) to orotic acid (OA) in the only redox reaction in *de novo* pyrimidine biosynthesis. DHODH enzymes are divided into two families based upon amino acid sequence and cellular localization [17] (Figure 1-4). Family 1A and 1B enzymes are located in the cytosol, whereas Family 2 enzymes possess an extended N-terminal helical domain which promotes enzyme association with membranes in prokaryotes [18], or attaches the enzyme to the inner mitochondrial membrane in eukaryotes [19]. Family 1 is further classified according to oligomeric state, co-factor composition, and the terminal electron acceptor involved in the complete reaction cycle. Family 1A enzymes are flavin mononucleotide (FMN)-containing homodimers of the *PyrDA* gene product which transfer electrons to fumarate. Family 1B enzymes are heterotetrameric,

contain FMN in the *PyrDB* gene product subunit, flavin adenine dinucleotide (FAD) and an iron-sulfur cluster in the *PyrK* gene product subunit, and utilize oxidized nicotinamide adenine dinucleotide (NAD^+) as the terminal electron acceptor [20]. Family 2 enzymes are monomeric and utilize FMN to transfer electrons to ubiquinone (CoQ), chemically coupling pyrimidine biosynthesis to the respiratory chain [21]. The CoQ binding site is thought to be formed by the extended N-terminal helical domain, which is unique to the Family 2 enzymes.

The phylogenetic distribution of DHODH enzymes does not follow any unifying rules [17]. Mammals, plants, and many gram-negative bacteria possess Family 2 enzymes. Some yeast, eubacteria, and protozoa have Family 1 enzymes, while others contain Family 2 enzymes. *Lactococcus lactis* is the only organism to date found to possess both a Family 1A and Family 1B enzyme [22].

The *P. falciparum* enzyme belongs to Family 2 and has been shown to be localized to the parasite mitochondrion [23, 24], where it utilizes ubiquinones with hydrophobic tails composed of eight or nine prenyl units (CoQ_8-CoQ_9) as terminal electron acceptors [25]. The malarial enzyme is predicted to contain a mitochondrial localization signal at the N-terminus and a 22 amino acid transmembrane domain (amino acids 143 – 165). Homologs such as human DHODH also encode a mitochondrial localization signal immediately prior to the transmembrane domain, and kinetic and structural studies of both enzymes have

focused on recombinant enzymes truncated after the predicted N-terminal transmembrane domain [26-30].

The X-ray structures of DHODH from several species have been reported [18, 27, 31-33], including the structure of truncated *P. falciparum* DHODH (*Pf*DHODH) which was solved in complex with orotic acid, FMN, and the inhibitor A77 1726 [34] (Figure 1-5). The orotate binding site of Family 2 DHODH enzymes is well conserved across species (Figure 1-6). Based on the competition of CoQ with A77 1726, the A77 1726 binding site is speculated to be the CoQ binding site as well [30]. This site is not as conserved between enzymes from different species, and a number of potent and species-selective inhibitors of the malarial enzyme that compete at this site have been identified [35]. The inhibitor/CoQ binding site is formed by two α-helices, which, in the primary amino acid sequence, lie between the predicted N-terminal transmembrane domain and the canonical β/α barrel domain. These α-helices are contiguous with the predicted transmembrane domain and are therefore likely to be adjacent to the surface of the inner mitochondrial membrane.

Catalytic Reaction

The reductive DHODH reaction, where enzyme-bound FMN is reduced as DHO is converted to OA, varies to some degree across the classes of DHODH enzymes, though the DHO site is generally well conserved. Structurally, the Family 1A enzymes use the same site for both DHO and fumarate catalysis.

Family 1B DHODH shuttles electrons from the distinct DHO site to FMN on the *PyrDB* subunit, then to the iron-sulfur cluster, the FAD, and ultimately the co-substrate NAD^+ on the *PyrK* subunit. Family 2 enzymes appear to possess two distinct co-substrate binding sites for DHO and ubiquinones, though no crystal structure exists co-crystallized with any electron acceptors.

While the DHO catalytic site is well conserved across species, a notable difference is the active site base used for proton abstraction from DHO. Family 1 enzymes use a cysteine residue whereas in Family 2 enzymes the active site base is a serine [36, 37]. The reaction mechanism for DHO catalysis has been explored in considerable detail for all classes of DHODH enzymes. Of particular interest to some groups is whether scission of the two DHO C-H bonds occurs in a stepwise or concerted fashion, and this has been explored using deuterium-labeled DHO as a substrate. The Family 1A enzyme from *Lactococcus lactis* [38] and the Family 1B enzyme from *Clostridium oroticum* [39] were found to reduce enzyme-bound FMN in a concerted mechanism, while the Family 1A enzyme from *Crithidia fasciculata* utilizes a stepwise reaction [40]. The two Family 2 enzymes studied to date, the *E. coli* and human enzymes, display a stepwise mechanism for flavin reduction [41]. These results suggest no unifying theme may be made regarding the mechanism of flavin reduction in regards to the active site base.

Mutational analysis of the DHO catalytic site has been performed on DHODH enzymes from all classes, both on the active site base and on residues

within the binding site thought to be involved in substrate binding and catalysis. The results of these studies show the active site base, whether it is cysteine (Family 1 enzymes) or serine (Family 2 enzymes), to be the lone residue responsible for proton abstraction from DHO [36-38, 42]. These studies have also shown that replacing the native active site base with the other type (serine to cysteine or cysteine to serine) greatly reduces enzyme activity. Mutational studies on the Family 1A enzyme from *L. lactis* have revealed that mutation to alanine of conserved residues can alter both co-substrate binding and catalysis of DHO [37].

The oxidative half-reaction, where enzyme-bound FMN is oxidized and electrons are transmitted to the terminal electron acceptor, is necessarily different for each class of DHODH enzyme due to the different electron acceptors used. As mentioned above, the Family 1A enzymes share a binding site for both DHO and fumarate co-substrates. The electron acceptor site for the Family 1B enzymes is contained on the *PyrK* subunit. For Family 2 enzymes, the electron acceptor site is thought to be on the opposite side of FMN as the DHO site, and reports have described the Family 2 enzymes to possess two physically and kinetically isolated catalytic sites [43]. These substantial differences between electron acceptor sites have precluded comparison of the oxidative half-reaction across different classes of DHODH enzymes. Perhaps as a result, the DHODH oxidative half-reaction has received little study. In one study, the DHOD oxidative half-reaction was found to be rate-limiting for the Family 1A *L. lactis* and Family 2 *E. coli* enzymes but not

rate-limiting for the Family 1B *L. lactis* enzyme [44]. Two other studies on the Family 2 bovine and *E. coli* enzymes show differing results. Using menadione as an electron acceptor, the oxidative half-reaction was found to be rate-limiting at low pH for the bovine enzyme but rate-limiting at high pH for the *E. coli* enzyme [42, 45]. The effect of mutagenesis on the oxidative half-reaction is limited to work performed in the Phillips lab on *Pf*DHODH [35] and one study on the human enzyme that used scanning alanine mutagenesis of all enzyme histidines [46]. There are therefore no proposed mechanisms for electron transfer to the terminal electron acceptor of any class of DHODH enzyme.

Inhibitors

Inhibitors of DHODH enzymes include DHO co-substrate analogues such as 5-fluoroorotate and benzoic acid derivatives [26, 47]. Although the DHO co-substrate site is well conserved, these compounds display both species and enzyme-class variability in inhibition. Species-selective inhibitors of the Family 2 enzymes have been discovered [48-50], and they form the basis of antimalarial drug design efforts [35]. These inhibitors bind in the extended N-terminal helical domain of Family 2 DHODH enzymes where the ubiquinone binding site is believed to be [27, 33, 34], and steady-state kinetic analysis shows them to be competitive toward ubiquinone substrates [26, 30, 51]. However, the relative positions of inhibitors and ubiquinone co-substrates remains to be adequately resolved [51].

PROJECT AIMS

Current Knowledge

The *de novo* pyrimidine biosynthesis pathway is a potential drug target in *Plasmodium falciparum*. DHODH is the drug target of leflunomide (Arava®) in the treatment of rheumatoid arthritis. Species-selectivity between the human and *Plasmodium falciparum* enzymes has been found for a series of drug-like compounds [35].

While the reductive half-reaction of DHODH enzymes has been studied extensively, the oxidative half-reaction has received little attention. There are few reports on electron transfer from FMN to terminal electron acceptors in Family 2 enzymes, which are limited to pH effects and the presence or absence of product orotate [42, 45]. More importantly, the ubiquinone binding site has not been revealed by structural studies. Inhibitors which show competitive inhibition toward ubiquinone co-substrates have been identified [30, 35], though some kinetic studies actually call into question the relative positions of these inhibitors and ubiquinone co-substrates [51]. As such, the location of the ubiquinone binding site is only inferred from a few kinetic studies which show competitive inhibition by inhibitors that have been co-crystallized with the enzyme, namely A77 1726 [30, 34].

Project Aims

The goals of this project are to define *Pf* DHODH residues responsible for ubiquinone co-substrate binding and catalysis. On the assumption that the ubiquinone binding site is shared with inhibitors, identification of the above residues will also help to define the determinants for inhibitor binding and species-specificity between the human and *Plasmodium* enzymes. The mechanism of inhibition by ubiquinone site inhibitors will also be revealed by these studies.

FIGURES

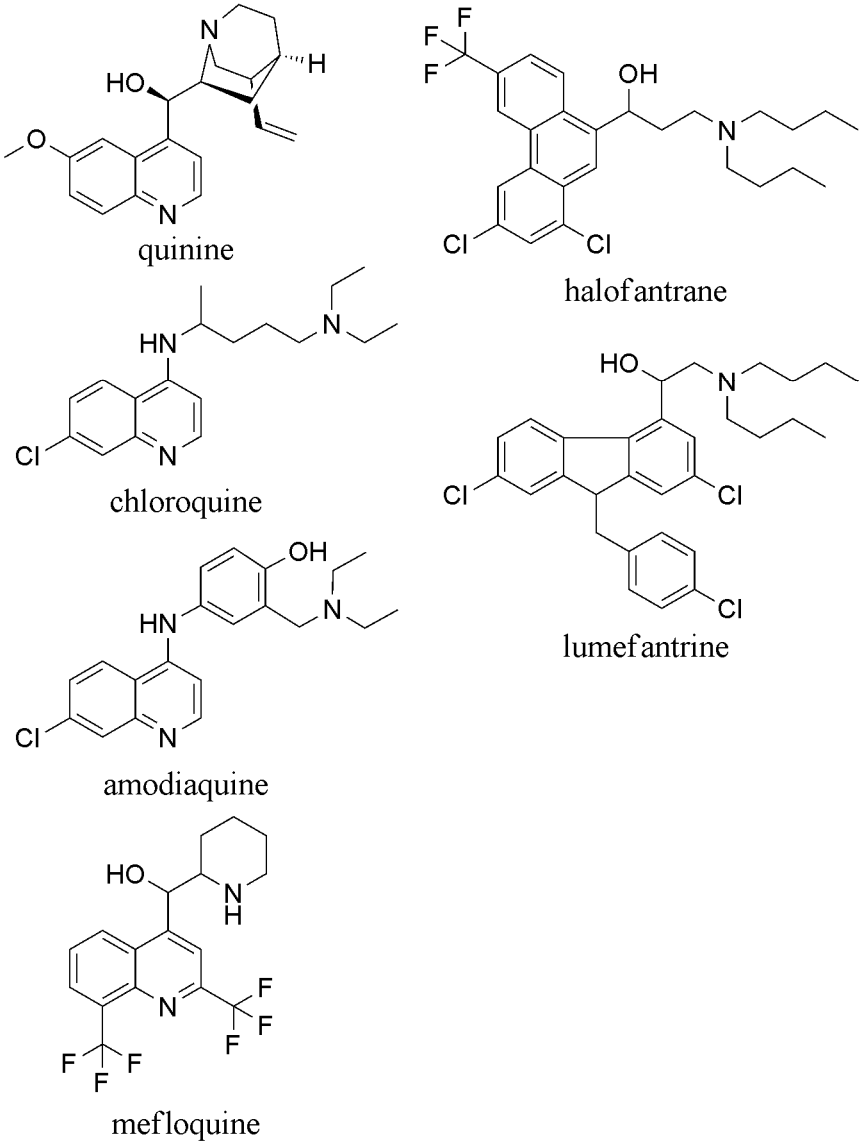

Figure 1-1 Quinoline antimalarials.

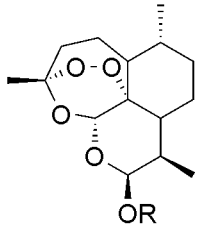

R=H	dihydroartemisinin
R=Me	artemether
R=Et	arteether
R=$CO(CH_2)_2CO_2H$	artesunate

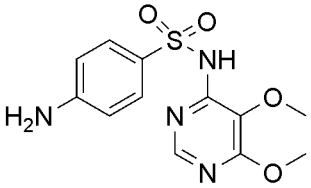

sulfadoxine

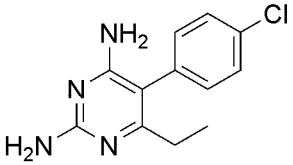

pyrimethamine

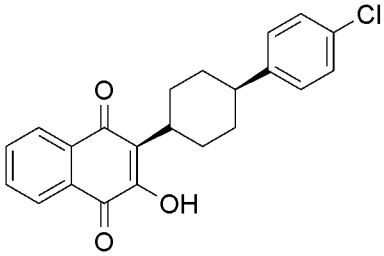

atovaquone

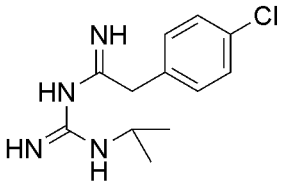

proguanil

Figure 1-2 Additional antimalarials.

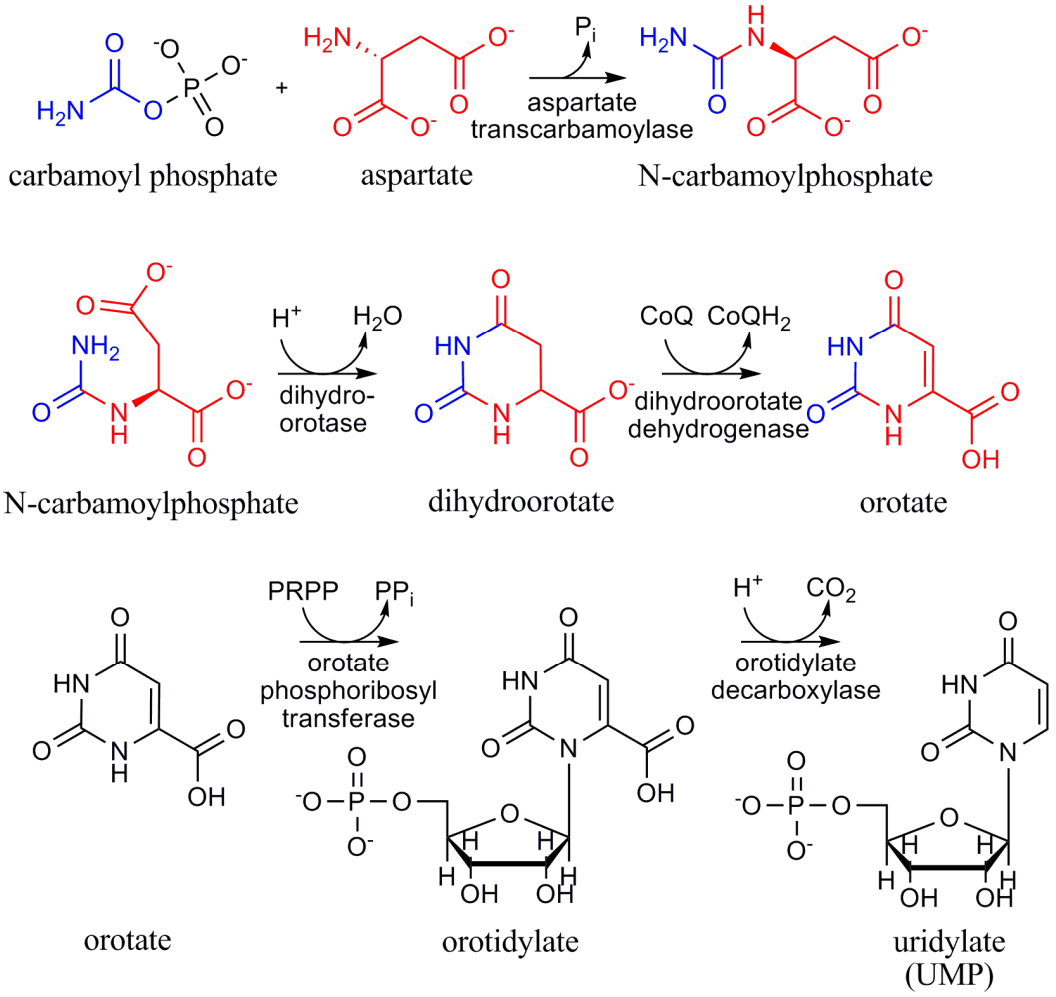

Figure 1-3 Pyrimidine biosynthesis pathway. Atoms colored blue are derived from glutamate and atoms colored red are derived from aspartate.

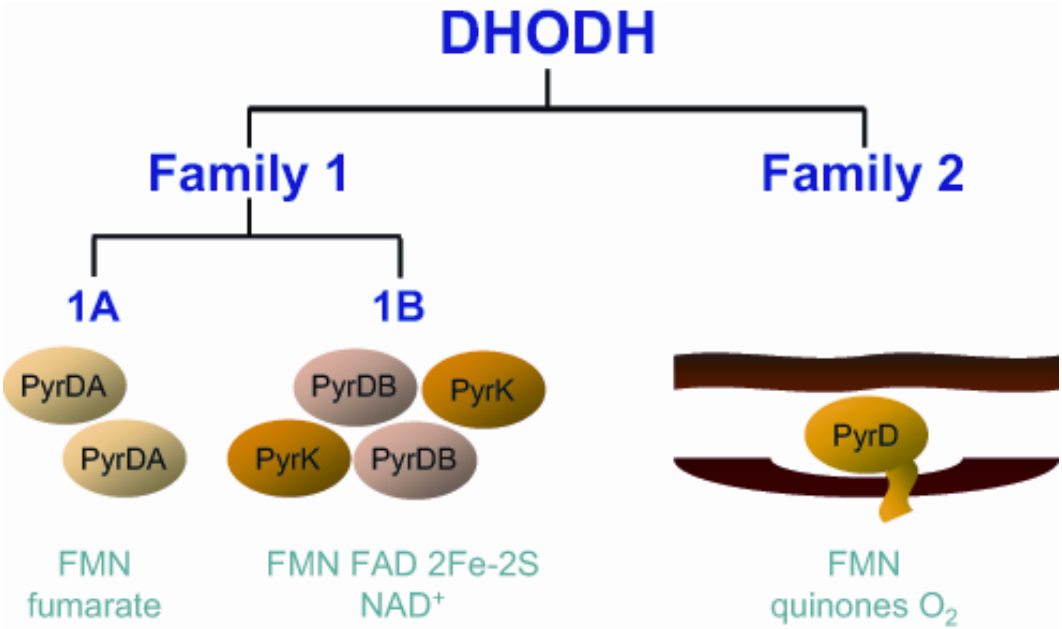

Figure 1-4 DHODH family of enzymes.

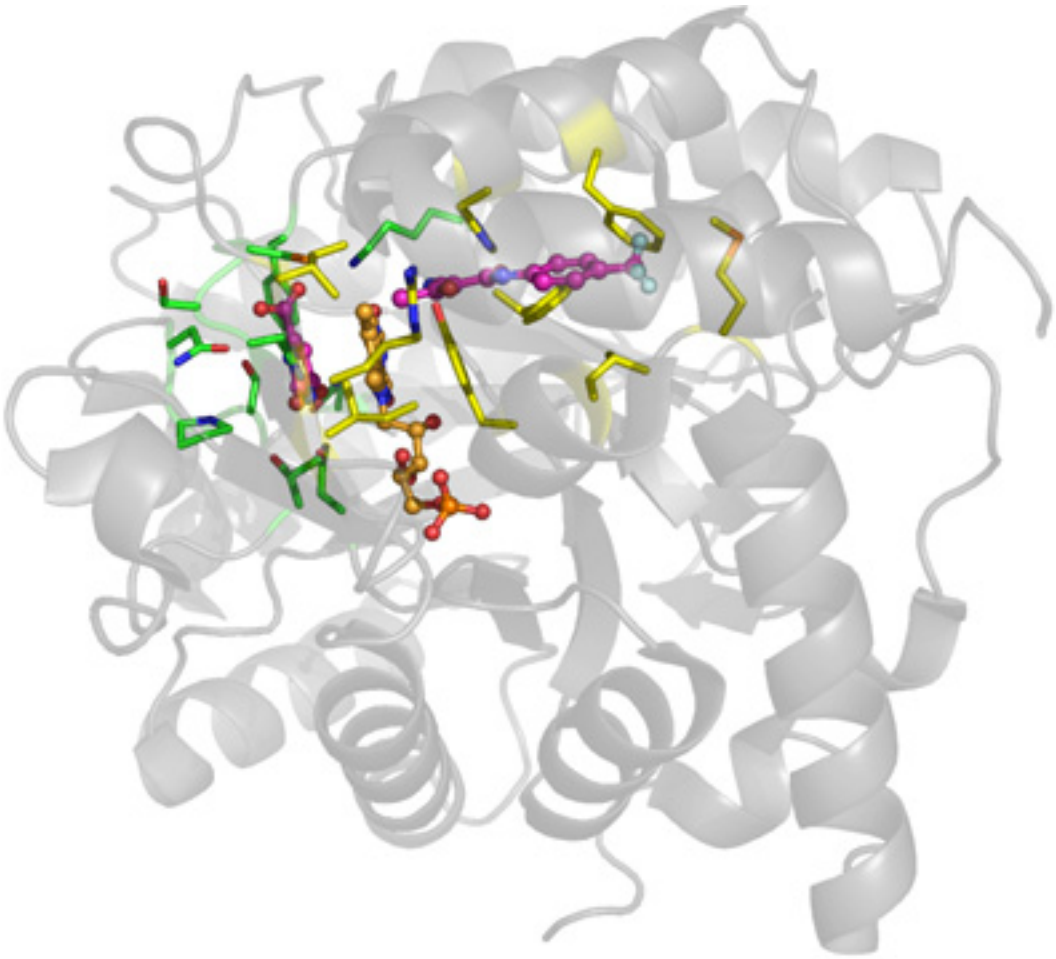

Figure 1-5 Active site of *Pf* DHODH with bound orotate and A77 1726. Cartoon of the enzyme backbone is in gray, nitrogen atoms are colored blue, oxygen atoms red, fluorine atoms light cyan. FMN is colored orange, orotate and A77 1726 are colored magenta. Residues in green are within 4 Å of orotate. Residues in yellow are within 4 Å of A77 1726 and chosen for mutation in these studies. Structure is from 1TV5.

```
E. coli   2                MYYPFVRKAL FQLDPERAHE FTFQQLRRIT GTPFEALVRQ
PfDHODH   158    FESYNPEFF LYDIFLKFCL KYIDGEICHD LFLLLGKYN- -----ILPYD
Rat       38               YAEYLMPGLQ RLLDPESAHR LAVRVTSLG- -----LLPRA
Human     30      MATGDERF YAEHLMPTLQ GLLDPESAHR LAVRFTSLG- -----LLPRA
                               ..       .* *  *  .                 *

E. coli   41    KVPA---KPV NCMGLTFKNP LGLAAGLDKD GECIDALGAM GFGSIEIGTV
PfDHODH   201   TSNDSIYACT NIKHLDFINP FGVAAGFDKN GVCIDSILKL GFSFIEIGTI
Rat       72    TFQDSDMLEV KVLGHKFRNP VGIAAGFDKN GEAVDGLYKL GFGFVEVGSV
Human     72    RFQDSDMLEV RVLGHKFRNP VGIAAGFDKH GEAVDGLYKM GFGFVEIGSV
                                 * ** .*.***.**  *  .*..    **. .*.*..

E. coli   88    TPRPQPGNDK PRLFRLVDAE GLINRMGFNN LGVDNLVENV KKAHY-----
PfDHODH   251   TPRGQTGNAK PRIFRDVESR SIINSCGFNN MGCDKVTENL ILFRKRQEED
Rat       122   TPQPQEGNPR PRVFRLPEDQ AVINRYGFNS HGLSVVEHRL RARQQKQAQ-
Human     122   TPKPQEGNPR PRVFRLPEDQ AVINRYGFNS HGLSVVEHRL RARQQKQAK-
                **. * ** . **.**  .   ..**  ***.  *   .   .    .

E. coli   133   ----DGVLGI NIGKNKDTPV EQGKDDYLIC MEKIYAYAGY IAINISSPNT
PfDHODH   301   KLLSKHIVGV SIGKNKDTV- -NIVDDLKYC INKIGRYADY IAINVSSPNT
Rat       171   LTADGLPLGI NLGKNKTSE- -DAAADYAEG VRTLGPLADY LVVNVSSPNT
Human     171   LTEDGLPLGV NLGKNKTSV- -DAAEDYAEG VRVLGPLADY LVVNVSSPNT
                       .*. ..**** .        *        .   * *  . .*.*****

E. coli   179   PGLRTLQYGE ALDDLLTAIK NKQNDLQAMH ---------- ----------
PfDHODH   349   PGLRDNQEAG KLKNIILSVK EEIDNLEKKN IMNDESTYNE DNKIGRYADY
Rat       225   AGLRSLQGKT ELRHLLSKVL QERDALKGT- ---------- ----------
Human     219   AGLRSLQGKA ELRRLLTKVL QERDGLRR-- ---------- ----------
                   *  *     *  ..  .     . *

E. coli   209   ---------- ---------- --HKYVPIAV KIAPDLSEEE LIQVADSLVR
PfDHODH   414   IAINNSHMMK DAKDNFLWFN TTKKKPLVFV KLAPDLNQEQ KKEIADVLLE
Rat       248   ---------- ---------- ---RKPAVLV KIAPDLTAQD KEDIASVARE
Human     247   ---------- ---------- --VHRPAVLV KIAPDLTSQD KEDIASVVKE
                                              . * *.****. ..   ..*

E. coli   237   HNIDGVIATN TTLDRSLVQG MKNCDQTGGL SGRPLQLKST EIIRRLSLEL
PfDHODH   449   TNIDGMIISN TTTQIN-DIK S-FENKKGGV SGAKLKDIST KFICEMYNYT
Rat       275   LGIDGLIVTN TTVSRPVGLQ GALRSETGGL SGKPLRDLST QTIREMYALT
Human     275   LGIDGLIVTN TTVSRPAGLQ GALRSETGGL SGKPLRDLST QTIREMYALT
                  ***.* .* **   .            **. **  *   **   *  .

E. coli   287   NGRLPIIGVG GIDSVIAARE KIAAGASLVQ IYSGFIFKGP PLIKEIVTHI
PfDHODH   497   NKQIPIIASG GIFSGLDALE KIEAGASVCQ LYSCLVFNGM KSAVQIKREL
Rat       325   QGRIPIIGVG GVSSGQDALE KIQAGASLVQ LYTALIFLGP PVVVRVKREL
Human     325   QGRVPIIGVG GVSSGQDALE KIRAGASLVQ LYTALTFWGP PVVGKVKREL
                ..***. * *. *   * * ** ****. * .*. . * *       .   .

E. coli
PfDHODH   547   NHLLYQRGYY NLKEAIGRKH -
Rat       375   EALLKERGFT TVTDAIGADH RR
Human     375   EALLKEQGFG GVTDAIGADH RR-
```

Figure 1-6 Structure-based sequence alignment of solved Family 2 DHOD enzymes. Sequences were hand-aligned according to residue location in the crystal structure. A star indicates complete conservation and a period indicates conservative substitution across the four sequences. Residues highlighted green are within 4 Å of orotate. Residues highlighted yellow are within 4 Å of A77 1726 in the human structure and chosen for mutation in these studies. Structures used were 1F76 (*E. coli*), 1TV5 (*P. falciparum*), 1UUM (rat), and 1D3H (human).

CHAPTER TWO
Detergent-Dependent Kinetics

INTRODUCTION

The *Pf* DHODH inhibitor/CoQ binding site is formed by two α-helices, which, in the primary amino acid sequence, lie between the predicted N-terminal transmembrane domain and the canonical β/α barrel domain. These α-helices are contiguous with the predicted transmembrane domain and are therefore likely to be adjacent to the surface of the inner mitochondrial membrane. Indeed, the α-helical residues with side-chains facing away from the enzyme and toward the lipid bilayer are hydrophobic and interact with bound detergent molecules in the X-ray structure (Figure 2-1). In contrast, polar and charged residues are oriented towards the β/α barrel domain and engage in hydrogen bonding or ionic interactions with other residue side-chains or backbone atoms.

The localization of malarial DHODH to the inner mitochondrial membrane and its requirement for a lipophilic substrate (CoQ) both suggest a kinetic model which takes into account catalysis at a surface-solution interface might be appropriate to describe the system. A number of groups have independently formulated schemes to describe catalysis in just such an environment [52-54]. One such reaction model describing interfacial kinetics was originally developed to characterize the activity of cobra venom phospholipase A_2 on mixed micelles composed of Triton X-100 and phosphatidylcholine [55]. This

model accounts for both the three-dimensional bulk interactions and two-dimensional surface interactions that occur between enzyme and substrate-detergent mixed micelles. Using this form of analysis, initial enzyme association with the substrate-detergent mixed micelle surface was kinetically separated from subsequent substrate binding and catalysis, and kinetic parameters that describe each process were individually derived. This kinetic approach has been utilized to describe a number of systems involving enzymes with hydrophobic or amphipathic substrates, products, activators, or inhibitors [52]. While the literature contains numerous examples of enzymes exhibiting surface dilution kinetics, these studies have been almost exclusively limited to lipid kinases, synthases, decarboxylases, phosphatases, and lipases acting upon lipid substrates [56]. Surface dilution kinetic analysis of ubiquinone-utilizing enzymes has so far been limited to the study of ubiquinol-cytochrome c reductase [57]. The dearth of investigation into ubiquinone analogue catalysis by these methods may be due to the finite solubility of these compounds compared to that of lipid substrates. The solubility of these compounds can limit the interpretation of individual experiments without careful consideration of the amounts of ubiquinone analogue present both in solution and micelle-bound.

In the studies presented here, I show N-terminal truncated *Pf* DHODH forms high molecular weight aggregates in the absence of detergent and demonstrate association of the enzyme with liposomes. I adopted an isothermal

titration calorimetry-based thermodynamic method to determine partitioning of ubiquinone analogues (Figure 2-2) into detergent micelles and found synthetic ubiquinone analogues with extended prenyl or alkyl tails (CoQ_2 and CoQ_D) partition into micelles while that with a short prenyl tail (CoQ_1) remains in solution. The truncated enzyme displays detergent-dependent activation up to the CMC of both Triton X-100 and Tween-80 and a subsequent decrease in activity at higher detergent concentrations, but only for substrates which partition into detergent micelles. Kinetic data of CoQ_D and CoQ_2 catalysis in substrate-detergent mixed micelles fit well to a surface dilution kinetic model and generated kinetic constants describing catalysis at the surface-solution interface. A kinetic characterization of this type has not been performed for any DHODH enzyme, and I discuss the advantages and limitations of such an analysis in regards to the use ubiquinone analogues in detergent micelles.

EXPERIMENTAL PROCEDURES

Materials

Buffer components, purified glucose oxidase (Type VII from *Aspergillus niger*) and catalase (from bovine liver), Brij 35, Triton X-100, and Tween-80 detergents and DHODH substrates L-DHO, DCIP, CoQ_1, CoQ_2 and CoQ_D were purchased from Sigma (St. Louis, MO) and were of the highest quality available. CHAPS detergent was purchased from Anatrace (Maumee, OH). Phosphatidylcholine (PC) and phosphatidylethanolamine (PE) were purchased

from Avanti Polar Lipids (Alabaster, AL). Size exclusion chromatography molecular weight standards were from Amersham Biosciences (Piscataway, NJ) or BioRad (Hercules, CA). All references to *P. falciparum* DHODH refer to the N-terminal truncated version unless specifically mentioned otherwise.

Methods

Protein Purification

Cloning, expression and purification of N-terminal truncated *Pf* DHODH were performed as described previously [26] with the modification that CHAPS detergent at 1% replaces Triton X-100 at 0.1% throughout protein purification.

Critical Micelle Concentration Determination

The CMC of each detergent in 50 mM HEPES, pH 8.0, 150 mM NaCl, and 10% glycerol was determined by the fluorometric 1,6-diphenyl-1,3,5-hexatriene method [58].

Analytical Gel Giltration

Gel filtration was performed on purified recombinant N-terminal truncated *Pf* DHODH using a Superdex 200 HR 10/30 analytical gel filtration column (Amersham Biosciences, Piscataway, NJ) calibrated with molecular weight standards. Gel filtration buffer was composed of 50 mM HEPES, pH 8.0, 150 mM NaCl, and 10% glycerol. High salt buffer contained 300 mM NaCl and no salt buffer omitted NaCl. Gel filtration buffer also contained various detergents when indicated. Enzyme was diluted to 2 mg/ml in the appropriate buffer before loading

on the column. Reported apparent molecular masses are the average ± SEM of at least duplicate experimental determinations.

Liposome Binding Experiments

Liposomes were produced by sonicating chloroform-removed PC and PE lipids with gel filtration buffer (50 mM HEPES, pH 8.0, 150 mM NaCl, and 10% glycerol) until an opalescent solution was produced. Purified recombinant N-terminal truncated *Pf* DHODH was mixed with either 10 mM (each) PC and PE mixed liposomes or gel filtration buffer and dialyzed against gel filtration buffer using dialysis tubing with a 12-14 kDa molecular weight cut-off. Dialyzed samples were applied to a Superose 6 HR 10/30 size exclusion column (Amersham Biosciences, Piscataway, NJ) calibrated with molecular weight standards, eluted at 0.5 ml/min, absorbance (light scattering for liposomes) at 280 nm was monitored, and 1 ml fractions were collected. *Pf* DHODH activity of each fraction was assayed at 25°C using the traditional colorimetric 2,6-dicholorindophenol (DCIP) assay at 600 nm ($\varepsilon = 18.8\ mM^{-1}\ cm^{-1}$) [59] by the addition of 25 µl of each fraction to a 0.5 ml reaction containing 0.5 mM L-DHO and 0.12 mM DCIP in gel filtration buffer containing 0.1% reduced Triton X-100. Data from one representative liposome binding experiment are presented.

Isothermal Titration Calorimetry (ITC)

Partitioning of synthetic CoQ analogues into Tween-80 micelles was examined at 37°C using a VP-ITC microcalorimeter (Microcal Corp,

Northampton, MA). The buffer was composed of 50 mM HEPES, pH 8.0, 150 mM NaCl, 10% glycerol, and 1% DMSO. Heats of injection were measured for 28 successive 10 µl injections of 5 mM Tween-80 into 100 µM synthetic CoQ analogue. All data were baseline corrected by subtracting the heat of dilution of a 5 mM Tween-80 titration into buffer only. Calorimetry data were fitted by nonlinear least squares to a partitioning model (described below) to obtain the change in enthalpy of partitioning (ΔH) and the partitioning coefficient (K) using the ORIGIN 7.0 software package. Partitioning experiments were performed at least three times and combined data ± SEM are reported.

Partitioning Model

Observing partitioning by high sensitivity ITC was originally developed for studying amphipathic molecules partitioning into lipid membranes [60]. Models have since been developed that describe both partitioning into membranes as well as membrane solubilization [61]. I have adapted the partitioning model to describe partitioning of lipid-like CoQ analogues into detergent micelles. As the models have been derived previously [62, 63], I present only a brief explanation relevant to our adaptation of the models. Partitioning equilibrium can be described using a partition coefficient (K) to relate the concentration of CoQ free in solution ($C_{Q,f}$) to the CoQ-to-detergent mixed micelle ratio (X_b) by $X_b = K \cdot C_{Q,f}$. The ratio X_b is equivalent to $n_{Q,b}/n_D^0$, that is, the molar amount of micelle-bound CoQ ($n_{Q,b}$) divided by the total molar amount of micellar detergent (n_D^0). As these molar

amounts are contained within the same volume (V_{cell}), the corresponding concentrations ($C_{Q,b}$ and C_D^0) can be used to describe X_b as $X_b = C_{Q,b}/C_D^0$. Conservation of mass ($C_Q^0 = C_{Q,b} + C_{Q,f}$) allows one to describe partitioning equilibrium as in Equation 2-1. During a partitioning experiment the CoQ concentration in the cell (C_Q^0) is fixed while the detergent concentration changes as detergent micelles are injected into the calorimeter cell. The first derivative of Equation 2-1 with respect to detergent concentration yields Equation 2, which is the expression for the change in micelle-bound CoQ ($\delta C_{Q,b}$) upon injection of detergent. In the calorimeter cell, $\delta n_{Q,b} = \delta C_{Q,b} \cdot V_{cell}$, and if the entire partitioning reaction is characterized by a ΔH of partitioning, a single injection of detergent results in the heat described by Equation 2-3, the partitioning model.

Enzyme Kinetic Assays

DHODH kinetic assays were performed at 25°C in 50 mM HEPES, pH 8.0, 150 mM NaCl, and 10% glycerol. L-DHO concentration was held constant at 0.5 mM throughout detergent-dependent, surface concentration-dependent, and surface dilution kinetic experiments. Steady-state measurements of orotic acid production were measured at 296 nm ($\varepsilon = 4.3$ mM^{-1} cm^{-1}). Reactions were performed under anaerobic conditions by depleting oxygen through the addition of 10 mg/ml glucose oxidase, 2 mg/ml catalase, and 50 mM glucose and incubation for 5 minutes prior to assay. Detergent-dependent kinetic studies were performed maintaining the individual CoQ concentration at 10 μM and varying

the concentration of Triton X-100 or Tween-80 detergent. Detergent-dependent oxidase activity was measured similarly by omitting glucose oxidase, catalase, and CoQ from the reaction mixture. Surface concentration-dependent kinetic assays were performed similar to detergent-dependent kinetic assays. Detergent concentrations were higher in these experiments such that detergent micelles were always present and the amount of free substrate was limited as much as experimentally possible. The various surface concentrations were produced by varying Tween-80 detergent concentration while holding CoQ concentration constant at several fixed values. Surface dilution kinetic assays were performed by simultaneously varying CoQ and micellar Tween-80 concentrations to produce various mole fraction isotherms along which the ratio of CoQ to micellar Tween-80 was maintained at several fixed values (1:50, 1:100, 1:200, and 1:400). Micellar Tween-80 was estimated as: $[\text{Tween-80}]_{\text{micellar}} = [\text{Tween-80}]_{\text{total}} - \text{CMC}$ of Tween-80 (12 μM). The mole fraction is obtained by: mole fraction of CoQ = $[\text{CoQ}] / ([\text{CoQ}] + [\text{Tween-80}]_{\text{micellar}})$. Specifically, the 1:51 mole fraction isotherm was produced with 100, 50, 10, and 5 μM CoQ in 5, 2.5, 0.5, and 0.25 mM micellar Tween-80, respectively. Other mole fraction isotherms were produced similarly: 50, 25, 5, and 2.5 μM CoQ (for 1:101); 25, 12.5, 2.5, and 1.25 μM CoQ (for 1:201); 12.5, 6.25, 1.25, and 0.625 μM CoQ (for 1:401) were mixed in 5, 2.5, 0.5, and 0.25 mM micellar Tween-80, from highest to lowest CoQ concentration within each mole fraction isotherm, respectively. Surface dilution kinetic data

were fitted individually to the Henri-Michaelis-Menten equation by nonlinear regression using the GraphPad Prism software package and globally to the surface dilution kinetic model [55] by nonlinear least squares analysis using the SigmaPlot software package. All experiments were performed in triplicate and combined data ± SEM are reported. Surface dilution kinetic data are presented with overlaid Henri-Michaelis-Menten curves.

Surface Dilution Kinetic Model

The surface dilution kinetic model is derived from descriptions of the two relevant kinetic steps [55]. In the bulk step (Scheme 2-1) enzyme (*E*) associates non-catalytically with the CoQ/Tween-80 mixed micelle (*A*) to form the enzyme-mixed micelle complex (*EA*). Formation of the complex is a function of the bulk concentration of both *E* and *A*. In surface dilution kinetics, *A* is defined as either the combined bulk concentration of detergent and CoQ substrate (in the "surface binding model") or as the bulk concentration of CoQ substrate alone (in the "substrate binding model") [55]. These two equation forms distinguish between a model ("surface binding") where enzyme initially associates non-productively with the general micelle surface versus a model ("substrate binding") where the enzyme directly associates with substrate on the micelle surface, albeit to form a non-productive complex. Scheme 2-2 illustrates the catalytic surface step, wherein the enzyme-mixed micelle complex *EA* binds an individual CoQ substrate (*B*) in the catalytic site. As this occurs at the micelle surface, the

association is a function of the surface concentrations of both *EA* and *B*, and *B* is therefore expressed in terms of mole fraction of CoQ in the mixed micelle. Catalysis then occurs, producing product (*P*) and regenerating *EA*. From these expressions, the surface dilution kinetics equation (Equation 2-4) is derived [55]. The apparent dissociation constant for the mixed micelle binding site is defined as $K_s^A = k_{-1}/k_1$ and is expressed in bulk concentration (molarity) units. The apparent interfacial Michaelis constant is defined as $K_m^B = (k_{-2}+k_3)/k_2$ and is expressed in surface concentration (mole fraction) units where the mole fraction of CoQ = [CoQ] / ([CoQ] + $[\text{Tween-80}]_{\text{micellar}}$). V_{max} is equal to the extrapolated V_{max} at infinite bulk concentration and unity mole fraction of CoQ substrate.

RESULTS

Analytical Gel Filtration of N-terminal Truncated Pf DHODH

Similar to other studies on Family 2 DHODH enzymes [27-30, 33], the *Pf* DHODH N-terminal predicted transmembrane domain was excluded from the *Pf* DHODH expression construct in an effort to produce a soluble enzyme for expression in *E. coli* [26]. However, the lipophilic nature of the CoQ substrate and the localization of the enzyme adjacent to the inner mitochondrial membrane suggest that the truncated enzyme may still have a significant hydrophobic surface that could associate with detergent molecules or promote protein aggregation. N-terminal truncated *Pf* DHODH (amino acids 169 - 569) was subjected to analytical gel filtration under a variety of conditions including

adjusting salt concentration and adding various detergents (Figure 2-3). These data show the 48 kDa truncated enzyme forms high apparent molecular weight aggregates regardless of NaCl concentration in the absence of detergent. In the presence of 0.1% Tween-80, 0.3% Brij 35, or 0.1% Triton X-100 detergents (68-, 25-, or 6-fold above their critical micelle concentrations (CMC), respectively), the apparent molecular weight is decreased relative to that found in the absence of detergent. The zwitterionic detergent CHAPS was tested at 0.1%, 0.5%, and 1% (0.27-, 1.4-, and 2.7-fold the detergent's CMC, respectively). While large protein aggregates appear in the absence of detergent micelles (i.e., in 0.1% CHAPS), increasing detergent concentration beyond the CMC (0.5 or 1% CHAPS) decreases the apparent molecular weight of *Pf* DHODH, eventually approaching that representative of monomeric *Pf* DHODH. The apparent molecular masses are a function of the Stokes' radius of the enzyme-detergent micelle complex and not strictly indicative of an absolute mass.

Association of N-terminal Truncated Pf DHODH with Liposomes

To determine if the hydrophobic regions exposed on truncated *Pf* DHODH are sufficient for membrane association, gel filtration experiments were performed in the presence of liposomes. *Plasmodium* parasite membranes are composed of primarily phosphatidylcholine (PC, 40-50%) and phosphatidylethanolamine (PE, 35-45%) [64]. Accordingly, to mimic the parasite membranes I utilized 1:1 mixed PC/PE liposomes for these interaction studies. *Pf*

DHODH was incubated with either PC/PE liposomes or buffer and subjected to dialysis. Dialyzed samples were then separated on a size exclusion column and fractions were assayed for *Pf* DHODH activity (Figure 2-4). Free liposomes elute in the column void volume due to their extended size. Enzyme incubated with buffer elutes in two fractions: a minor active component, likely composed of large protein aggregates, elutes near the void volume, while the major active component elutes with a smaller apparent molecular mass (Figure 2-4). In contrast to enzyme incubated with buffer, enzyme incubated with PC/PE liposomes elutes in a single active peak corresponding to the elution profile of free PC/PE liposomes (Figure 2-4).

Partitioning of Synthetic CoQ Analogues into Tween-80 Micelles

To determine if synthetic ubiquinone analogues partition into detergent micelles, partitioning was examined by isothermal titration calorimetery. Triton X-100 has traditionally been used in the kinetic analysis of mitochondrial DHODH [26-30, 33]. However, for these studies a different non-ionic detergent, Tween-80, was employed because it has a lower CMC (relative to Triton X-100), which allowed lower concentrations of detergent to be used in the partitioning experiments and lower concentrations of CoQ to be studied in the kinetic studies described below. Tween-80 micelles were injected into the calorimeter cell containing synthetic CoQ analogue (100 μM), and the heat of each injection was recorded. After subtracting the heat from a blank titration of detergent into buffer,

the heat from each individual injection was plotted and fitted to the partitioning model described above (Equation 2-3). The data reveal a positive but decreasing heat of injection as Tween-80 micelles are titrated into CoQ_2 and CoQ_D consistent with an endothermic partitioning model (Figure 2-5). The partitioning model fit the data with the parameters: for CoQ_2, K = 31.8 mM^{-1}, ΔH = 1.29 kcal/mol; for CoQ_D K = 16.1 mM^{-1}, ΔH = 1.30 kcal/mol, where K represents a forward partitioning coefficient relating the free CoQ concentration to the mole fraction of CoQ bound in micelles. In contrast to the significant endothermic process observed for CoQ_2 and CoQ_D, injection of CoQ_1 into Tween-80 micelles yielded a much smaller change in enthalpy and the overall process was exothermic (K = 1.69 mM^{-1}, ΔH = -0.469 kcal/mol). These data suggest that the chemical process associated with the change in enthalpy for CoQ_1 may be of a different nature than for the longer-chain substrates. Together, these results support the conclusion that CoQ_2 and CoQ_D partition into Tween-80 micelles while the short-chain CoQ_1 either does not partition or may only weakly associate with Tween-80 micelles.

Detergent-dependent Activity of N-terminal Truncated Pf DHODH

The detergent-dependence of *Pf* DHODH catalysis was examined for each of the synthetic ubiquinone analogues in both Triton X-100 and Tween-80. DHODH is also able to use molecular oxygen as the terminal electron acceptor for the reaction, thus the oxidase activity served as a control to monitor the catalytic behavior of the enzyme with a substrate that is not specifically present at

the surface-solution interface. Oxidase activity shows only a minor general dependence on detergent concentration, with activity increasing by approximately 15% when Triton X-100 or Tween-80 are included in the reaction, however, the concentration of detergent required to fully stimulate the oxidase activity is below the CMC of either detergent (Figure 2-6a). The activity of *Pf* DHODH toward CoQ_1 displays similar trends with a gradual 2-fold increase in rate observed as the concentration of either detergent is increased (Figure 2-6b). Again, no significant dependence on the detergent CMC can be detected in the CoQ_1 activity. The finding that both oxidase activity and activity with CoQ_1 are modestly lower in the absence of detergent may result from the formation of less active protein aggregates, which were shown to form in the absence of detergent in analytical gel filtration experiments (Figure 2-3), or may be due to some form of substrate-specific activation by monomeric detergent molecules. In contrast to the results for oxidase and CoQ_1 activity, *Pf* DHODH CoQ_2 activity displays both activation at low detergent concentrations and a subsequent decrease in activity at higher detergent concentrations (Figure 2-6c). The activation phase peaks at the CMC of each detergent (Triton X-100 CMC ≈ 250 μM, Tween-80 CMC ≈ 12 μM, by our determination) and activity decreases thereafter. *Pf* DHODH detergent-dependent CoQ_D activity is even more pronounced than CoQ_2 activity, displaying a very sharp distinction between the activation phase below the CMC of each detergent and the decrease in activity above each detergent CMC (Figure 2-6d).

Surface Concentration-dependent Kinetics of N-terminal Truncated Pf DHODH

The surface concentration dependence of *Pf* DHODH activity toward CoQ_2 and CoQ_D was examined at several fixed molar CoQ concentrations under conditions where detergent micelles are always present and no more than 3% of CoQ substrate exists in the aqueous phase. *Pf* DHODH activity under these conditions displays the same saturable surface concentration dependence regardless of bulk substrate concentration (Figure 2-7).

Surface Dilution Kinetic Analysis of N-terminal Truncated Pf DHODH

A more thorough analysis of the kinetics of *Pf* DHODH was performed using CoQ_1, CoQ_2, and CoQ_D in Tween-80 micelles. Tween-80 was chosen over Triton X-100 because its lower CMC allowed lower CoQ concentrations to be used when maintaining constant fixed ratios of detergent to CoQ. *Pf* DHODH activity was determined as a function of CoQ_1 concentration at four fixed mole fractions of CoQ_1 in Tween-80 micelles (Figure 2-8a). For CoQ_1, *Pf* DHODH activity does not change considerably as the mole fraction of CoQ_1 in Tween-80 micelles is varied over an 8-fold range. These data fit well to a simple Henri-Michaelis-Menten solution steady-state kinetic model. In contrast, *Pf* DHODH activity toward CoQ_2 in Tween-80 micelles demonstrates increasing activity as the mole fraction of CoQ_2 is increased relative to Tween-80 over the 8-fold range tested (Figure 2-8b). The same behavior is exhibited toward CoQ_D in Tween-80 micelles, though *Pf* DHODH CoQ_D activity is generally lower than corresponding

CoQ_2 activity (Figure 2-8c). In both CoQ_2 and CoQ_D mixed Tween-80 micelles, activity is saturable and the effect of varying the mole fraction of CoQ substrate is primarily seen in an altered V_{max} with little change in K_m^{app}, as evidenced by the Henri-Michaelis-Menten curves presented in Figure 2-8.

Analysis of the detergent-dependent kinetic data for *Pf* DHODH on CoQ_2 and CoQ_D according to the surface dilution kinetic model described in Equations 4-6 provides a very good fit to the data. The bulk step of the surface dilution kinetic model can be expressed in terms of "surface binding", which describes an initial (non-productive) enzyme association with the general micelle surface, or in terms of "substrate binding", where enzyme associates (again, non-productively) directly with the substrate presented on the micelle surface. *Pf* DHODH CoQ_2 and CoQ_D activity data were fitted by global analysis to both models, and the resulting parameters are displayed in Table 1. The CoQ_2 and CoQ_D data fit both the "surface binding" and "substrate binding" models with similar r-squared values, thus the data do not distinguish between them. The surface dilution kinetic parameters for CoQ_2 and CoQ_D mixed Tween-80 micelles utilizing the "surface binding" model versus the "substrate binding" model yielded similar V_{max} values and K_m^B values. The apparent dissociation constant K_s^A compares the concentration of mixed detergent plus CoQ required to achieve one-half V_{max} in the "surface binding" model and to the concentration of CoQ alone required to achieve one-half V_{max} in the "substrate binding" model. Thus the difference in

magnitude of the K_s^A term in the two models is simply a reflection of how the term is defined. The data for CoQ_1 in mixed Tween-80 micelles did not fit either surface dilution kinetic model.

DISCUSSION

Eukaryotic Family 2 DHODH enzymes associate with the inner mitochondrial membrane where they utilize ubiquinone, a lipophilic molecule possessing a multi-prenyl unit tail, as the terminal electron acceptor in the reaction. Accordingly, both enzyme and substrate are constricted to the lipid bilayer, poised to carry out catalysis at the surface-solution interface. As with other Family 2 enzymes, *Pf* DHODH contains both a putative transmembrane domain and an extended helical domain N-terminal to the catalytic domain. *Pf* DHODH truncated after the predicted transmembrane domain was expressed to produce a soluble enzyme amenable to kinetic characterization. Analytical gel filtration of the truncated enzyme in either the absence of detergent or the presence of sub-CMC (monomer) detergent revealed protein oligomer formation (Figure 2-3) suggesting the presence of exposed hydrophobic residues which could promote association of the enzyme with lipid bilayers. In support of this hypothesis, physical association of *Pf* DHODH with PC/PE mixed liposomes was demonstrated by size exclusion chromatography (Figure 2-4).

I examined the partitioning of three synthetic ubiquinone analogues by isothermal titration calorimetry and found two analogues which partition

appreciably into detergent micelles and one which does not (Figure 2-5). This is, to our knowledge, the first thermodynamic examination of ubiquinone analogues partitioning into detergent micelles. Given the partitioning coefficients one is able to calculate the amount of free and micelle-bound substrate under any experimental condition. This is an important consideration when using substrates which have finite solubility in solution. Using these three ubiquinone analogues one is able to produce environments in which substrates are differentially present either free in solution or in a substrate-detergent mixed micelle (Tables 2a and 2b).

Various surface dilution kinetic models have been developed to describe both obligate and facultative interfacial catalysis [52-54]. An obligate interfacial kinetic model was developed to describe phospholipase A_2 catalysis in a processive "scooting" mode [53]. This system requires the production of well defined lipid substrate vesicles and the demonstration of irreversible enzyme association with those vesicles. This approach has worked well for studies of phospholipase A_2, where that enzyme has been shown to associate irreversibly with model liposomes and utilize essentially insoluble phospholipids as substrates. I have been unable to demonstrate strictly irreversible *Pf* DHODH association with liposomes, and the ubiquinone analogues I investigated possess varying degrees of solubility in aqueous solution (by design), making this obligate interfacial kinetic regime both unapproachable and undesirable for our system.

Furthermore, because *Pf* DHODH is able to use molecular oxygen and the soluble CoQ_1 substrate as terminal electron acceptors, a purely obligate interfacial kinetic model would not be appropriate for this enzyme.

An alternate model, initially developed to describe the activity of cobra venom phospholipase A_2 towards phospholipids in substrate-detergent mixed micelles, does not discriminate between obligate and facultative interfacial kinetics [55]. Kinetic analysis of *Pf* DHODH is approachable using substrate-detergent mixed micelles (as opposed to substrate vesicles, which have not been described for synthetic ubiquinone analogues), and I have therefore chosen to analyze the kinetics of *Pf* DHODH in substrate-detergent mixed micelles. By utilizing the nonionic detergent Tween-80 instead of the traditional Triton X-100 for these studies, I was able to sample a suitable range of substrate concentrations and substrate-to-detergent mole fraction ratios to produce a comprehensive surface dilution kinetic description of the *Pf* DHODH enzyme. Additionally, the use of substrate-detergent mixed micelles and ubiquinone analogues which partition into detergent micelles to varying degrees has allowed me to produce environments in which substrate is differentially present at the surface-solution interface (CoQ_2 and CoQ_D) or in the aqueous phase (CoQ_1).

Substrate-detergent mixed micelles have traditionally been produced using essentially insoluble lipid substrates. Certain limitations arise when employing ubiquinone analogues that partition into detergent micelles to varying degrees and

have finite solubility in solution. As noted above, the partitioning behavior produces a finite amount of these ubiquinone analogues in the aqueous phase and the free substrate concentration is inversely proportional to the concentration of detergent. Therefore, simple detergent-dependence experiments do not distinguish between utilization of free, micelle-bound, or both pools of substrate and do not alone demonstrate surface dilution kinetic behavior. Nonetheless, experimental conditions can be designed to minimize the amount of free substrate. Additionally, the amount of substrate in either pool can be determined by calculation in an effort to ascertain the catalytically relevant substrate pool. The combined observations of a potential surface dilution phase, a similar dependence on surface concentration across a range of bulk substrate concentrations, and a fit to the full surface dilution kinetic model together provide evidence that interfacial kinetic behavior is being observed.

To examine whether *Pf* DHODH catalyzes the reaction at the surface-solution interface, kinetic characterization of *Pf* DHODH detergent-dependent activity towards synthetic ubiquinone analogues was undertaken. The study revealed a biphasic kinetic dependence on detergent concentration, but only for analogues that were demonstrated to partition into detergent micelles (CoQ_2 and CoQ_D) (Figure 2-6). Accordingly, enzyme activity was equally dependent upon the surface concentration of CoQ_2 and CoQ_D over a range of bulk substrate concentrations (Figure 2-7). Further examination of *Pf* DHODH kinetic behavior

over a broad range of CoQ concentrations and CoQ/Tween-80 mixed micelle compositions demonstrated that a kinetic model that accounts for surface dilution was appropriate to explain the enzyme activity toward CoQ_2 and CoQ_D (Figure 2-8). This kinetic behavior is consistent with catalysis of the longer-chain ubiquinone analogues at the micelle surface [65, 66]. Although the CoQ analogues do have finite solubility in aqueous solution, the free longer-chain CoQ analogue concentrations are low (at most 0.63 or 1.2 μM at 100 μM CoQ_2 or CoQ_D, respectively; Table 2-2b). Furthermore, along any particular mole fraction isotherm the free CoQ_2 or CoQ_D concentrations are nearly constant. Thus, changes in free CoQ concentration are unlikely to account for the increase in rate that is observed as total CoQ concentration is increased. While some variation in free CoQ concentration is observed if the concentrations are compared across mole fraction isotherms, plotting of the catalytic rate versus free CoQ concentration demonstrates that the data do not fit a simple Henri-Michaelis-Menten model. Thus, a model in which enzyme catalyzes the reaction in solution solely on the limited free CoQ available in this phase is not supported by the data.

The kinetic data for CoQ_2 and CoQ_D fit well to the surface dilution kinetic model developed to characterize the activity of cobra venom phospholipase A_2 towards phospholipid substrate in Triton X-100 mixed micelles [52, 55]. This model accounts for both the three-dimensional bulk interactions and two-dimensional surface interactions that occur between enzyme and substrate,

allowing kinetic constants to be determined that reflect the true nature of the enzyme-substrate interactions. This model has also been used to study several other lipid-dependent enzymes: phosphatidylserine synthetase from *E. coli* [67], phosphatidylinositol 4-kinase from *S cerevisiae* [65, 68], *Arabidopsis* phospholipase Dδ [66], and beef heart ubiquinol-cytochrome c reductase [57]. The detergent-dependent kinetics (Figure 2-6) [66-69], surface concentration-dependent kinetics (Figure 2-7) [70], and the surface dilution kinetics (Figure 2-8) [65, 66] of *Pf* DHODH are similar to that found for these other systems, supporting the conclusion that *Pf* DHODH catalyzes the reduction of longer-chain ubiquinones at the two dimensional surface-solution interface, where the catalytically relevant substrate pool for these analogues exists. Thus, for substrates (and potentially inhibitors) which partition into the micelle a kinetic model that accounts for catalysis at a surface-solution interface may be most appropriate to fully describe the system.

The surface dilution kinetic model has been useful in describing the regulation (both inhibition and activation) of yeast phosphatidate phosphatase by both soluble and hydrophobic molecules by defining substrate concentration in terms of surface concentration [71-73]. The studies presented here have established meaningful kinetic constants and suggest suitable bulk and surface concentration ranges to employ in the future analysis of potential regulatory molecules of this class of enzymes. The results also suggest more soluble

substrates may be utilized in an effort to minimize the detergent-dependence of catalysis and simplify the analysis of regulatory molecules. Moreover, these studies establish the importance of understanding the differential catalytic behavior that can be observed based upon the use of different substrates and detergent concentrations.

The full surface dilution kinetic analysis of a ubiquinone-dependent enzyme has been very limited [57], and the detergent dependence of the reaction kinetics has not been previously reported for any dihydroorotate dehydrogenase. Our results suggest that this phenomenon may be wide-spread in this class of enzymes, and thus should be an important consideration in the kinetic analysis of any ubiquinone-dependent enzyme. Furthermore, this type of analysis might also be appropriate for additional classes of enzymes that utilize hydrophobic or amphipathic substrates beyond the lipid-utilizing enzymes to which surface dilution and interfacial kinetic analysis has primarily been limited. However, these studies emphasize the importance of understanding the behavior of substrates with variable solubility in the presence of detergent micelles.

Altogether, these results lead to the conclusion that truncated *Pf* DHODH contains a membrane interaction site that allows the enzyme to associate both with substrate-detergent mixed micelles and with liposomes in the absence of the predicted hydrophobic transmembrane domain. This property is reminiscent of the *E. coli* DHODH enzyme, which lacks a transmembrane domain and associates

with membranes solely via interactions with the extended N-terminal α-helical domain [19]. The catalytic domain of DHODH is composed of a β/α barrel and an extended N-terminal domain composed of two additional α-helices between which the inhibitor A77 1726 binds [34]. Although no DHODH structures to date include co-crystallized ubiquinone, kinetic data suggests the inhibitor utilizes an overlapping binding site with ubiquinone [30]. The α-helical residues that surround this site and face the inner mitochondrial membrane *in vivo* are exclusively hydrophobic and aromatic residues (Figure 2-1). Charged and polar residues are generally oriented toward the β/α barrel domain and engage in ionic interactions or hydrogen bonding with other side-chain or backbone atoms. Indeed, the *Pf* DHODH structure contains two C_8E_5 detergent molecules; one detergent molecule packs against hydrophobic residues F171 and F174 and the other engages in hydrogen bonding with K173. These structural insights combined with our kinetic data suggest that the *Pf* DHODH ubiquinone binding site is likely to be partially buried in the lipid bilayer, and that while the transmembrane domain may serve as a membrane anchor, the functionally important interaction relative to the catalytic cycle occurs at the extended N-terminal α-helical domain.

Malaria DHODH is the focus of significant effort to identify new chemotherapeutic approaches against the parasite [26, 34, 35, 74-76], including the recent identification of potent and selective inhibitors that bind the putative

CoQ site by high-throughput screening [35]. The finding that the enzyme interacts with ligands at the surface-solution interface has implications in directing future drug discovery efforts. Compounds should have the necessary chemical characteristics that permit effective interaction with this hydrophobic binding site.

EQUATIONS

$$C_{\mathrm{Q,b}} = \frac{K \cdot C_{\mathrm{D}}^{0}}{1 + K \cdot C_{\mathrm{D}}^{0}} \cdot C_{\mathrm{Q}}^{0}$$

Equation 2-1 Partitioning equilibrium.

$$\delta C_{\mathrm{Q,b}} = \frac{K \cdot C_{\mathrm{Q}}^{0}}{\left(1 + K \cdot C_{\mathrm{D}}^{0}\right)^{2}} \cdot \delta C_{\mathrm{D}}^{0}$$

Equation 2-2 Partitioning equilibrium upon detergent addition.

$$\delta h_{\mathrm{i}} = \Delta H \cdot V_{\mathrm{cell}} \cdot \frac{K \cdot C_{\mathrm{Q}}^{0}}{\left(1 + K \cdot C_{\mathrm{D}}^{0}\right)^{2}} \cdot \delta C_{\mathrm{D}}^{0}$$

Equation 2-3 Partitioning model.

$$V = \frac{V_{\max}[A][B]}{K_{s}^{A} K_{m}^{B} + K_{m}^{B}[A] + [A][B]}$$

Equation 2-4 Surface dilution kinetic equation.

SCHEMES

$$E + A \underset{k_{-1}}{\overset{k_1}{\rightleftharpoons}} EA$$

Scheme 2-1 Bulk step.

$$EA + B \underset{k_{-2}}{\overset{k_2}{\rightleftharpoons}} EAB \xrightarrow{k_3} EA + P$$

Scheme 2-2 Surface step.

TABLES

	substrate binding model		
	V_{max} (s^{-1})	K_s^A (μM)	K_m^B (mole %)
CoQ_2	14.4 ± 0.3	7.0 ± 1.9	0.094 ± 0.021
CoQ_D	7.4 ± 0.4	7.0 ± 2.0	0.32 ± 0.08
	surface binding model		
	V_{max} (s^{-1})	K_s^A (μM)	K_m^B (mole %)
CoQ_2	16.4 ± 0.2	890 ± 80	0.18 ± 0.01
CoQ_D	9.1 ± 0.5	520 ± 90	0.63 ± 0.10

Table 2-1 Surface dilution kinetic values for *Pf* DHODH. The substrate binding model defines the mixed micelle binding site as the CoQ concentration and the surface binding model defines it as the combined concentrations of CoQ and Tween-80. V_{max} is the extrapolated V_{max} at infinite substrate concentration and unity mole fraction of CoQ substrate, K_s^A is the apparent dissociation constant for the mixed micelle binding site, and K_m^B is the apparent interfacial Michaelis constant.

Tween-80 (mM)	fraction of micelle-bound CoQ		
	CoQ_1	CoQ_2	CoQ_D
5.00	0.90	0.99	0.99
2.50	0.81	0.99	0.98
0.50	0.46	0.94	0.89
0.25	0.30	0.89	0.80

Table 2-2a Fraction of micelle-bound CoQ at various detergent concentrations. The concentration of micelle-bound CoQ ($C_{Q,b}$) at any given concentration of added CoQ (C_Q^0) is expressed as the fraction of micelle-bound CoQ ($C_{Q,b}/C_Q^0$). Values were calculated from the partition coefficients and the detergent concentrations using Equation 2-1.

	free CoQ_2 (μM) at mole fraction				free CoQ_D (μM) at mole fraction			
total CoQ	1:51	1:101	1:201	1:401	1:51	1:101	1:201	1:401
highest	0.63	0.31	0.16	0.078	1.2	0.61	0.31	0.15
-	0.62	0.31	0.16	0.078	1.2	0.61	0.30	0.15
-	0.59	0.30	0.15	0.074	1.1	0.55	0.28	0.14
lowest	0.56	0.28	0.14	0.070	1.0	0.50	0.25	0.12

Table 2-2b Concentration of free CoQ under surface dilution kinetics conditions. The concentrations of CoQ free in solution under the experimental conditions given in Figure 2-8 were calculated from Table 2-2a. Total CoQ concentrations used for each mole fraction isotherm were: 100, 50, 10, 5 μM (1:51); 50, 25, 5, 2.5 μM (1:101); 25, 12.5, 2.5, 1.25 μM (1:201); 12.5, 6.25, 1.25, 0.625 μM (1:401).

FIGURES

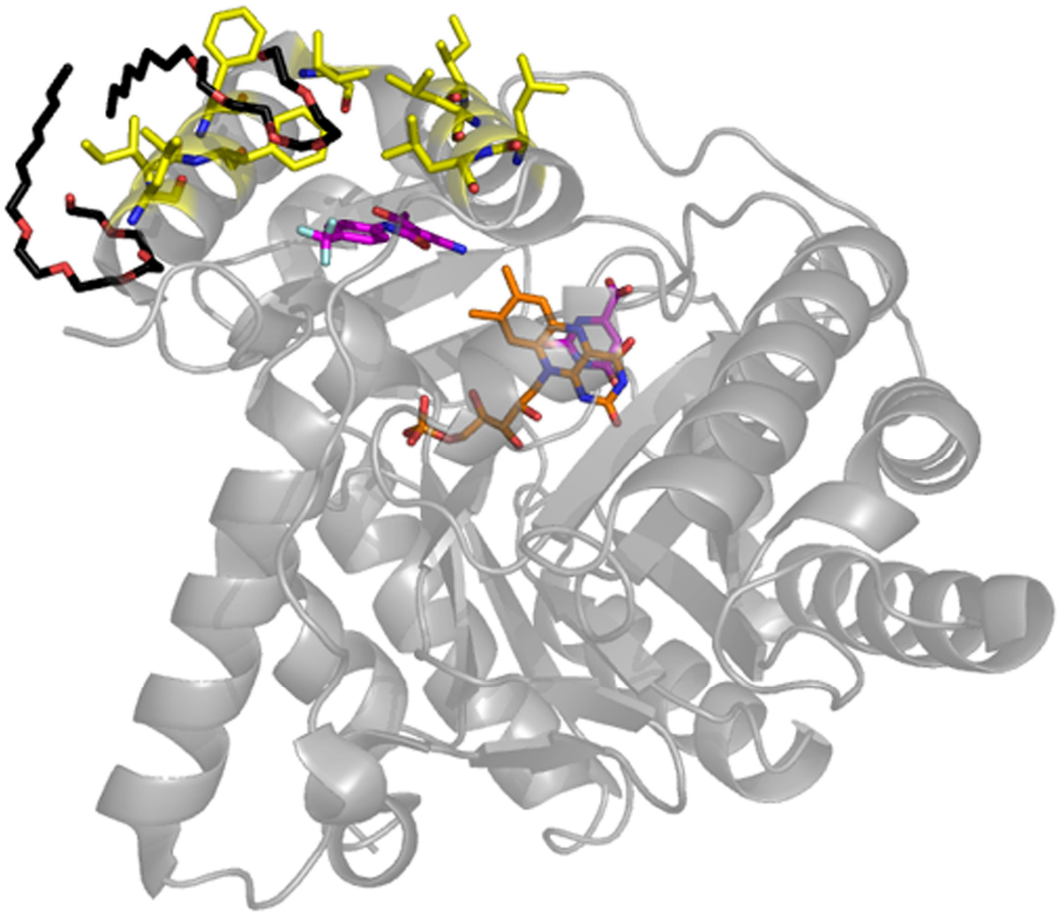

Figure 2-1 Hydrophobic helices in *Pf* DHODH. The structure is displayed as a ribbon diagram in transparent gray. Oxygen is red, nitrogen is blue, and fluorine is cyan. Orotic acid and A77 1726 are colored magenta, FMN is colored orange, detergent molecules C_8E_5 are colored black. Hydrophobic residues extending from the two N-terminal α-helices are colored yellow (the left helix contains residues L167, I170, F171, and F174; the loop contains I179; the right helix contains I183, L187, L190, and L191). The image was produced using PyMOL (DeLano Scientific, San Francisco, CA) from structure coordinates 1TV5 [34].

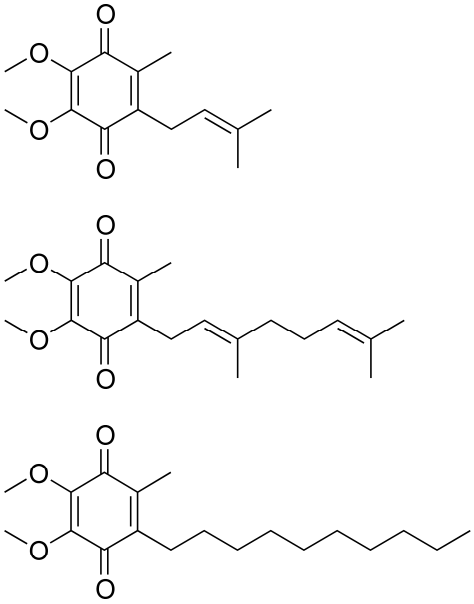

Figure 2-2 Synthetic ubiquinone analogues. CoQ_1 (top), CoQ_2 (middle), and CoQ_D (bottom). CoQ_1 contains a single isoprene unit tail, CoQ_2 a geranyl tail, and CoQ_D an unsaturated decyl tail.

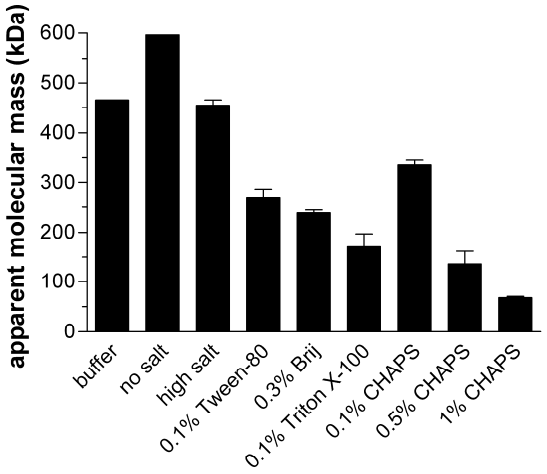

Figure 2-3 Apparent molecular mass from analytical gel filtration of *Pf* DHODH under various conditions. Buffer contained 50 mM HEPES, pH 8.0, 150 mM NaCl, 10% glycerol. High salt and no salt refer to the same buffer containing 300 mM or 0 mM NaCl. Detergent additions to the above buffer are indicated. The expected molecular mass of *Pf* DHODH is 48 kDa. Error bars represent the standard error of the mean for at least duplicate determinations.

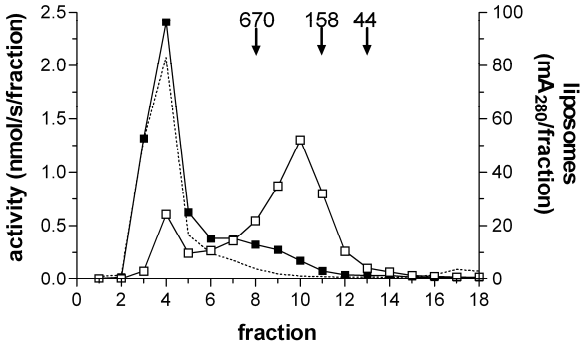

Figure 2-4 Size exclusion chromatography of *Pf* DHODH and PC/PE liposomes. Light scattering of free PC/PE liposomes was monitored by absorbance at 280 nm (dashed line). Enzyme was mixed with PC/PE liposomes (solid squares) or buffer (open squares), dialyzed, and subjected to size exclusion chromatography. The activity of each fraction was determined by colorimetric DCIP assay. The elution volume of molecular mass standards thyroglobulin (670 kDa), bovine gamma globulin (158 kDa), and chicken ovalbumen (44 kDa) are indicated with arrows. Data from one representative experiment are shown.

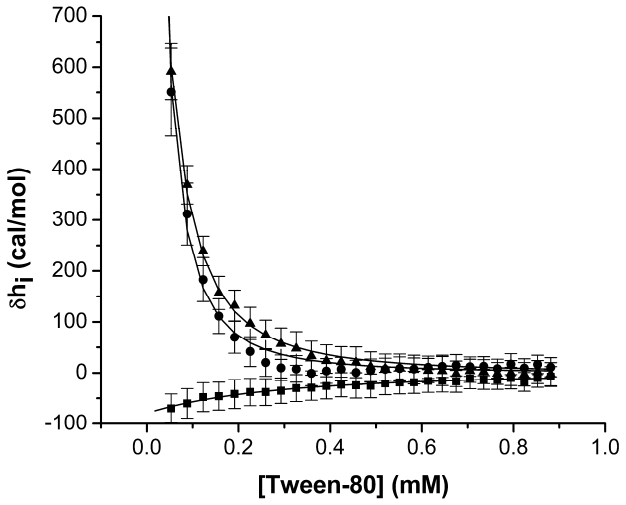

Figure 2-5 Titration of synthetic CoQ analogues with Tween-80 micelles. The heat of injection of Tween-80 into CoQ_1 (squares), CoQ_2 (circles), or CoQ_D (triangles) was measured by isothermal titration calorimetry. Error bars represent the standard error of the mean for triplicate determinations. Data were fitted to the partitioning model. The parameters were K = 1.69 mM^{-1}, ΔH = -0.469 kcal/mol (CoQ_1); K = 31.8 mM^{-1}, ΔH = 1.29 kcal/mol (CoQ_2); K = 16.1 mM^{-1}, ΔH = 1.30 kcal/mol (CoQ_D).

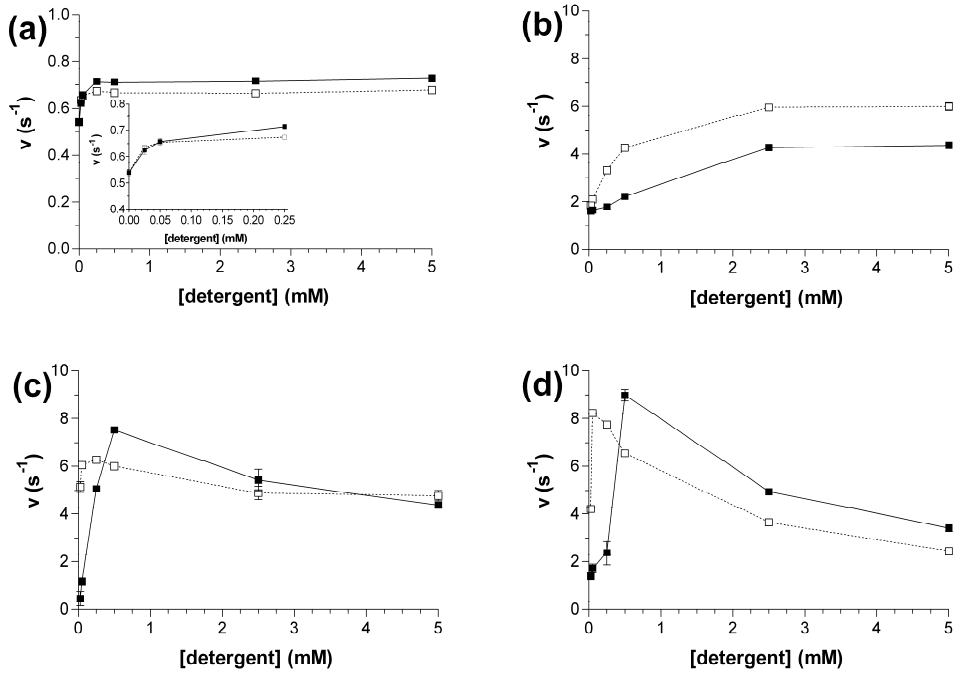

Figure 2-6 Detergent-dependent activity of *Pf* DHODH towards oxygen and synthetic CoQ analogues. (a) Oxygen-, (b) CoQ_1-, (c) CoQ_2-, and (d) CoQ_D-dependent activity. CoQ concentrations were held constant at 10 μM while the concentration of either Triton X-100 (solid squares, solid line) or Tween-80 (open squares, dashed line) was varied. Error bars represent the standard error of the mean for triplicate determinations.

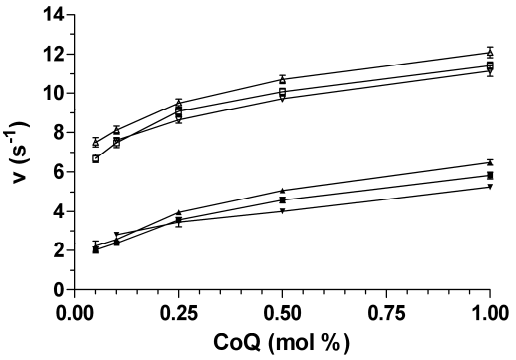

Figure 2-7 Surface concentration-dependent activity of *Pf* DHODH towards CoQ_2 and CoQ_D. The surface concentration of CoQ was varied by adjusting Tween-80 detergent concentration while holding bulk CoQ_2 (open symbols) or CoQ_D (closed symbols) concentration constant at 20 μM (squares), 30 μM (triangles), and 40 μM (inverted triangles). Error bars represent the standard error of the mean for at least duplicate determinations.

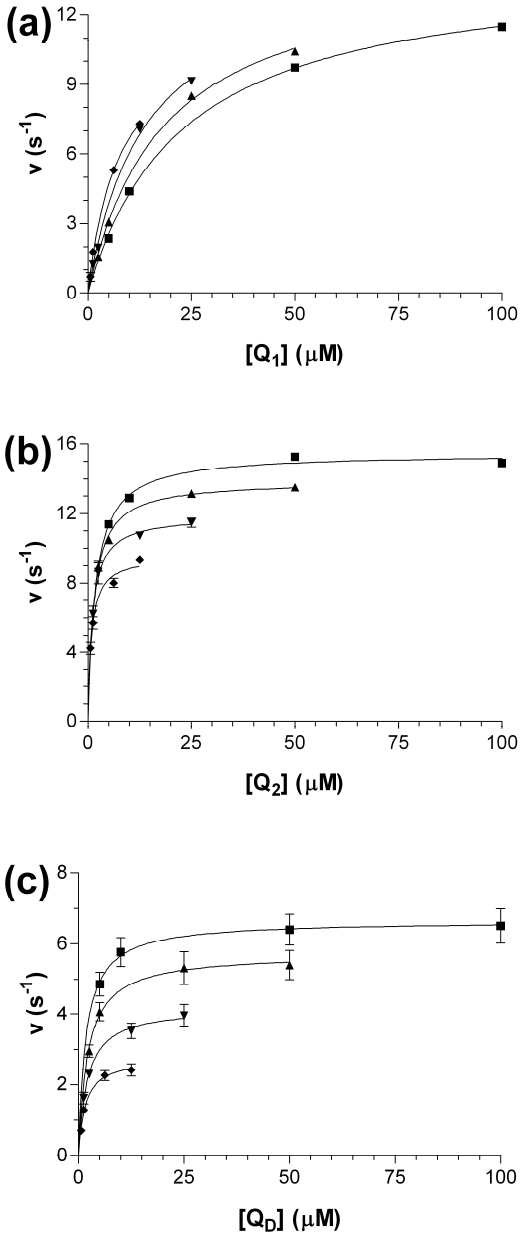
(a)
v (s-1)
[Q1] (μM)
(b)
v (s-1)
[Q2] (μM)
(c)
v (s-1)
[QD] (μM)

Figure 2-8 Activity of *Pf* DHODH toward CoQ in the presence of Tween-80 micelles. The mole fraction ratio of CoQ to micellar Tween-80 was held constant at 1/51 (squares), 1/101 (triangles), 1/201 (inverted triangles), or 1/401 (diamonds) by varying Tween-80 concentration along with (a) CoQ_1, (b) CoQ_2, or (c) CoQ_D concentration. Detergent and substrate concentrations used are noted in the text. Error bars represent the standard error of the mean for triplicate determinations. Curves represent nonlinear fit of the data to the Henri-Michaelis-Menten equation. Data are plotted according to the "substrate binding model," where *A* is defined as the bulk concentration of CoQ and is plotted on the abscissa.

CHAPTER THREE
Mutational Kinetic Analysis

INTRODUCTION

We previously identified a number of potent, species selective inhibitors of *P. falciparum* DHODH by high-throughput screening, including N-(3,5-dichloro-phenyl)-2-methyl-3-nitro-benzamide (DCPMNB; Figure 3-1), and demonstrated that these inhibitors bind to the same site as A77 1726 by mutagenesis of the binding pocket [35]. The structural basis for the observed species selectivity is evident through comparison of the x-ray structures of the human and malarial enzymes, which show that the A77 1726 binding-site is highly variable in amino acid sequence between the enzymes from the two species (Figure 3-2) [26, 27, 34].

Kinetic analysis of the patterns of inhibition of both mammalian and *Pf* DHODH have suggested that some, but not all, of the inhibitors that bind to the A77 1726 binding-site are competitive with CoQ [30, 33, 35, 48, 50, 51, 75]. Brequinar and A77 1726 have been observed to bind to almost fully overlapping sites in the crystal structure of the human enzyme, yet non-competitive inhibition towards CoQ is observed for A77 1726 and competitive inhibition has been observed for Brequinar [27, 51]. These results have led to the hypothesis that CoQ binds to the A77 1726/brequinar binding-site. However, because no structural

data are available for CoQ bound to DHODH of any species, the location of the CoQ binding-site remains speculative and controversial.

The reductive half-reaction, where DHO is converted to OA, has been examined in considerable detail for both Family 1 and 2 enzymes by steady-state and pre-steady-state approaches. Further, the literature contains extensive data on the amino acid residues involved in the reaction at the DHO binding-site [38, 41, 42, 77]. In contrast, the oxidative half-reaction where FMN is re-oxidzed by CoQ remains poorly studied. In order to provide insight into the position of the CoQ binding-site relative to inhibitors of *Pf* DHODH I utilized site-directed mutagenesis of the A77 1726 binding-site and analyzed the effects of these mutations on both the steady-state reaction and the oxidative and reductive half-reactions by pre-steady-state kinetic methods using single wavelength stopped-flow spectroscopy. The data provide insight into the residues involved in electron transfer between CoQ and FMN, and they suggest inhibitors bind in a channel that blocks the path of electron flow, but does not significantly overlap with the CoQ binding-site.

EXPERIMENTAL PROCEDURES

Methods

P falciparum DHODH Cloning

The previously described *Pf* DHODH-pProEXHTa expression plasmid encoding amino acids 157–565 [26] was used as the cloning template. The *NdeI*

restriction site at nucleotide 595 (full-length DHODH numbering) was eliminated using the QuickChange site-directed mutagenesis kit (Strategene) as recommended by the manufacturer, where the forward primer was 5'-GAAAATATAATATATTACC**C**TATGATACTAGTAATGATAGTATATATGC-3' (altered base in bold). Next, *NdeI* and *XhoI* restriction sites were introduced by mutagenesis at the N and C-terminus of the *Pf* DHODH ORF where the forward primer was, 5'-AACCTGTATTTT**CATATG**TTTTTTGAATCTTATAATCC-3' and the reverse primer was 5'-CGTCGACCGTGT**CTCGAG**ACTTTTGCTATGCT-3'. The *NdeI-XhoI* DHODH fragment from the resulting plasmid was then subcloned into pET22b vector (Novagen) to generate the final expression construct (*Pf* DHODH-pET22b-1). The *Pf* DHODH ORF was sequenced in its entirety. Mutations of the A77 1726 binding site residues to Ala were created using the QuickChange kit with the following primers (forward only are shown).

H185A	5'-GTGAAATATGT**GCT**GACCTTTTTTTATTACTAGG-3'
F188A	5'-GAAATATGTCATGACCTT**GCT**TTATTACTAGG-3'
F227A	5'-GGTGTTGCTGCAGGA**GCT**GATAAAAACGG-3'
R265A	5'-CCACGTATTTTT**GCA**GACGTTGAATCTAG-3'
I272A	5'-CGTTGAATCTAGAAGT**GCT**ATAAATTCATGTGG-3'
Y528A	5'-GGTGCTTCAGTTTGTCAATTA**GCT**TCTTGTTTGG-3'
Y528F	5'-CAGTTTGTCAATTA**TTT**TCTTGTTTGG-3'

Y528W 5'-CAGTTTGTCAATTA**TGG**TCTTGTTTGG-3'

L531A 5'-CAGTTTGTCAATTATATTCTTGT**GCG**GTTTTTAATGG-3'

P falciparum DHODH Expression and Purification

BL21-DE3 *E coli* cells containing the appropriate wild-type or mutant *Pf* DHODH pET22b expression construct were grown in LB containing 100 mg/ml ampicillin overnight at 37°C. Large scale cultures (typically 6 liters) were inoculated with the overnight culture into LB broth with 10% glycerol and 100 mg/ml ampicillin and grown at 37°C to an OD_{600} of ~ 0.7. Protein expression was induced by the addition of isopropyl-beta-D-thiogalactopyranoside (IPTG; 200 μM), cultures were supplemented with FMN (100 μM) and grown at 16°C overnight. Cells were pelleted by centrifugation at 3000 x *g* at 4°C and the pellet re-suspended in 0.2 L lysis buffer (50 mM HEPES pH 8.0, 150 mM NaCl, 10 mM imidazole, 5 mM 2-mercaptoethanol, 100 μM FMN, 10% glycerol, and a protease inhibitor mixture consisting of phenylmethylsulfonyl fluoride (200 μM), leupeptin (1 μg/ ml), antipain (2 μg/ml), benzamidine (10 μg/ml), pepstatin (1 μg/ml), and chymostatin (1 μg/ml)). Triton X-100 (2% v/v) and lysozyme (1 mg/ml) were added, and the mixture was stirred on ice for one hour before freezing in liquid nitrogen. DNase (0.05 mg/ml) was added to the thawed lysate, the mixture was sonicated on ice until cleared and centrifuged at 20000 x *g* at 4°C.

The resulting supernatant was loaded onto a Ni-NTA column equilibrated in buffer A (50 mM HEPES pH 8.0, 150 mM NaCl, 20 mM imidazole, 5 mM 2-

mercaptoethanol, 100 μM FMN, 10% glycerol, 0.1% Triton X-100). The column was washed in buffer A until a stable baseline at A_{280} was reached, then bound enzyme was eluted with buffer B (50 mM HEPES pH 8.0, 150 mM NaCl, 300 mM imidazole, 5 mM 2-mercaptoethanol, 100 μM FMN, 10% glycerol, 0.1% Triton X-100). Fractions containing protein were pooled and concentrated with an Amicon Ultra centrifugal concentrating device (Amicon), desalted on a HiPrep 26/10 Desalting Column (Amersham Biosciences) equilibrated with enzyme assay buffer (50 mM HEPES pH 8.0, 150 mM NaCl, 10% glycerol, 0.1% Triton X-100) and re-concentrated as above.

Protein concentration was determined by Bradford analysis using bovine serum albumen as a standard. FMN concentration was determined by first heat denaturing the protein to release the bound cofactor (purified enzyme typically diluted to 1 – 20 μM), followed by measuring absorbance at 445 nm (ε_{445} = 12.5 mM^{-1} cm^{-1}) to calculate FMN concentration.

Circular Dichorism Spectroscopy

CD spectra were recorded for wild-type and mutant enzyme samples (8 μM protein) in 50 mM sodium phosphate pH 8.0. Spectra were collected from 190 to 260 nm using an Aviv CD Spectrometer Model 62DS at 25°C in quartz cuvettes (1 mm path length) with a five second integration time and three repetitions. Molar ellipticity data are presented as the average of the three readings versus buffer alone.

Steady-State Kinetics

Steady-state kinetic measurements were performed in enzyme assay buffer at 25°C. Production of orotic acid was observed directly at 296 nm (ε_{296} = 4.30 $mM^{-1}cm^{-1}$) when using both oxygen and ubiquinone analogs (CoQ_1 or CoQ_D) as terminal electron acceptors. When ferricyanide was used as the electron acceptor, the reduction of ferricyanide was observed at 420 nm (ε_{420} = 1 mM^{-1} cm^{-1}), taking into consideration two moles of ferricyanide are reduced per every one mole of DHO. For oxidase activity, DHO concentration (5–500 μM) was varied at a fixed enzyme concentration (100 nM). For CoQ and ferricyanide, assays were performed at a fixed concentration of DHO (0.5 mM), over a range of CoQ (1–100 μM) or ferricyanide (1–500 μM) concentrations in the presence of wild-type or mutant *Pf* DHODH (5–50 nM). Oxygen was depleted from these reactions through the addition of 0.1 mg/ml glucose oxidase, 0.02 mg/ml catalase, and 50 mM glucose, followed by incubation for 5 min prior to assay. Data were fitted to the Michaelis-Menten equation (Equation 3-3) to determine the steady-state parameters (k_{cat} and K_m).

Substrate-dependent DCPMNB inhibition experiments were performed with DHO (500 μM) and CoQ_1, CoQ_D, or ferricyanide (100 μM) or dissolved oxygen (~300 μM), 5–50 nM enzyme, and a range of inhibitor concentrations (10 nM–100 μM). Wild-type and mutant *Pf* DHODH IC_{50} values for DCPMNB were obtained from similar experiments using 500 μM DHO, 20 μM CoQ_D, 5 nM

enzyme and a range of inhibitor concentrations (10 nM–100 μM). Data were fitted to Equation 3-1 to determine the IC_{50}.

Pre-Steady-State Kinetic Analysis by Stopped Flow Spectroscopy

Rapid kinetic analysis was performed in enzyme assay buffer at 4°C on a Bio-Logic SFM-3 stopped flow instrument equipped with a 1 cm pathlength quartz cell, and controlled by BioKine 16 V 3.03 software. The calculated dead time was 4 ms at a flow rate of 15 ml/s. A wavelength of 485 nm was used to observe the transition of FMN between the oxidized and reduced state. For DHO-dependent reactions, enzyme (final concentration 20 μM) was mixed with a range of DHO concentration (final concentrations 63 to 1000 μM). CoQ_1-dependent experiments were performed under anaerobic conditions using the glucose oxidase and catalase system described above, as well as constant bubbling with nitrogen during sample preparation. For CoQ_1-dependent reactions, oxidized enzyme (45 μM) was reduced with a limiting amount of DHO (30 μM) under an atmosphere of nitrogen before loading on to the stopped flow instrument. Reduced enzyme (final concentration 10 μM) was then mixed with CoQ_1 (final concentrations 31 to 500 μM). A minimum of four reaction traces at each substrate concentration were recorded. The observed DHO- and CoQ_1-dependent reactions were fitted to an exponential equation to obtain k_{obs} (Equation 3-2) (BioKine 16 software). Two exponentials were required to obtain good fits (as measured by the residual plots) to the DHO-dependent half-reactions. One

exponential was sufficient to obtain good fits to the CoQ_1-dependent half-reaction. The resulting substrate-dependent fast phases ($k_{obs,1}$) displayed a hyperbolic dependence on substrate concentration and were fitted to Equation 3-3 to determine the $k_{red/ox}$ and K_d values for each half-reaction. Inhibition experiments were performed by pre-mixing enzyme (10 or 20 μM final concentration, as above) and inhibitor at a concentration sufficient to ensure complete occupancy of the DHODH inhibitor binding site (1 mM OA, 1 mM A77 1726, or 50 μM DCPMNB, final concentrations).

RESULTS

Analysis of the A77 1726 Binding Site

Residues within van der Waals distance of the inhibitor A77 1726 binding-site were identified in the x-ray structure of *Pf* DHODH. In total, fifteen residues are found within the 4 Å of A77 1726, and of these only five are conserved in sequence between human and *Pf* DHODH. To identify residues that participate in the energetics of CoQ and inhibitor binding, five highly conserved residues (H185, F227, R265, Y528 and L531) and two variable residues (I272 and F188) were selected for analysis by Ala mutagenesis (Figure 3-2). F227, Y528 and L531 were selected because they make up an aromatic/hydrophobic patch that bridges between A77 1726 and the FMN cofactor. H185 and R265 were chosen because they are the only charged residues that contact the ligand, and I272 and F188 were selected to assess the role of residues that are variable between

enzymes from different species. H185 also forms a bridging interaction between Y528 and F227. Site-directed mutagenesis was performed as described in Experimental Procedures, and the wild-type and mutant *Pf* DHODH enzymes were expressed in *E. coli* and purified by Ni^{+2}-agarose column chromatography.

FMN Content of Wild-type and Mutant Pf DHODH

The stochiometry of FMN to protein in the purified protein preparations was determined for each enzyme preparation. FMN content ranged from 90–40% for wild-type enzyme and 5–70% for mutants. Mutation of F227, I272, Y528, and L531 to Ala affected the FMN content most, resulting in mutant enzymes with 5–25% FMN. Attempts to reconstitute FMN into enzyme preparations containing low FMN levels by unfolding and re-folding with various urea and/or guanidine concentrations in the presence of excess FMN were unsuccessful. The addition of free FMN to a reaction mixture containing FMN-poor enzyme did not result in an increase in catalytic rate. For kinetic analysis, enzyme concentration was determined by FMN concentration, thus normalizing for only catalytically competent enzyme.

Evaluation of Wild-type and Mutant Pf DHODH by CD Spectroscopy

CD spectroscopy was used to examine the secondary structure fold characteristics of mutant enzymes in comparison to wild-type *Pf* DHODH (Figure 3-3). The CD spectra of wild-type and mutant enzyme are very similar, suggesting the mutant enzymes have similar secondary structure content to the wild-type

enzyme, and are thus not grossly misfolded. Additionally, these data demonstrate that even for preparations that contain sub-stochiometric FMN to protein content, the overall folding for both apo- and holo-enzyme is essentially indistinguishable at this resolution.

Steady-state Kinetic Analysis of Wild-type and Mutant Pf DHODH

Steady state kinetic analysis was performed on the wild-type and mutant enzymes in the presence of two ubiquinone analogues containing different length hydrophobic tails (CoQ_1 and CoQ_D (Table 3-1). CoQ_1 contains a single isoprenoid unit, while CoQ_D contains a longer alpiphatic tail (Scheme 3-1). These two substrates were previously demonstrated to have different detergent micelle partitioning behavior, with CoQ_1 remaining soluble and CoQ_D partitioning into detergent micelles [78]. Assays were performed in the presence of a glucose oxidase and catalase system to eliminate molecular oxygen from the reaction. For wild-type *Pf* DHODH the measured kinetic constants (K_m^{app} CoQ 11–13 μM; k_{cat} 8–12 s^{-1}) were similar for the two substrates. None of the Ala mutations had a significant effect on K_m^{app} for the CoQ substrate, with the largest affect (2–4-fold increase) being observed for the R265A mutation. Similarly, a modest reduction in k_{cat} was observed for most of the mutations (2–4-fold). However, mutation of Y528A caused a significant reduction in k_{cat} (40–100-fold respectively). The loss of activity upon mutation of Y528 could be partially restored by replacing the

Y528 with Phe or Trp, suggesting that an aromatic residue at this position plays a role in the reaction chemistry.

In the absence of CoQ substrates, molecular oxygen can function as the terminal electron acceptor to re-oxidize the FMN cofactor. The steady-state rates of this reaction were determined for dissolved O_2 present in buffers in the absence of the glucose oxidase and catalase system. Rates were determined for a range of DHO concentrations to determine the k_{cat} for the oxidase reaction (0.42 s^{-1} for the wild-type enzyme). This rate is 25–30-fold lower than the CoQ catalyzed steady-state rate (Table 3-1). Only the I272A and Y528A mutant enzymes had rates that were significantly lower than the wild-type enzyme (5- and 4-fold lower respectively).

Thus, the steady-state kinetic data demonstrate that mutation of the A77 1726 binding-site residues has little to no effect on the K_m^{app} for CoQ, suggesting that the CoQ binding-site may not overlap the A77 1726 site. However, because K_m is a reflection of multiple kinetic steps, and does not represent a true dissociation constant, effects on CoQ binding may be masked in the steady-state kinetic analysis. The finding that mutation of Y528 decreases the k_{cat} for the reaction suggest that this residues may play a catalytic role in the electron transfer between FMN and the oxidant. In order to determine more specifically which steps in the reaction pathway were being affected by the A77 1726 binding-site

mutations, the reductive and oxidative half-reactions were characterized by pre-steady state kinetic analysis.

Pre-steady-state Kinetic Analysis of the FMN Reductive Half-reaction

Enzyme-bound oxidized FMN displays two characteristic absorbance bands that diminish upon reduction and re-appear at red-shifted positions in the presence of the reaction product orotic acid after re-oxidization (Figure 3-4). The DHO-dependent reduction of FMN was monitored by single wavelength stopped-flow spectroscopy at 485 nm, an isosbestic point of oxidized and re-oxidized FMN in the presence of product orotate. Data were collected in the absence of CoQ, thus only a single turnover was observed during the course of the experiment. The rate of the reaction was too fast to be measured at 25°C, the temperature of the steady-state analysis. Preliminary analysis demonstrated that most of the reaction occurred during the mixing dead time (4 ms) at this temperature. Data were collected at 4°C to slow the reaction and at this temperature approximately 50% of the reaction occurred in the dead time for the highest substrate concentration. Absorbance data were collected over a 4–1000 ms time period for a range of DHO concentrations (63–1000 μM) and were fitted to Equation 3-2 to determine the observed rate constants for the reaction (k_{obs}). The data require two exponentials to obtain a good fit as demonstrated by the residual plots. The first observable kinetic phase ($k_{1,red}$) is dependent on DHO concentration and the data were fitted to Equation 3-3 to determine the kinetic

constants for this phase of the reaction (for the wild-type enzyme $K_{d,red}$ = 230 μM; $k_{1,red}$ = 350 s^{-1}) (Table 3-2, Figure 3-5, Scheme 3-2). Estimating an extinction coefficient difference of $\Delta\varepsilon_{485}$ = 5 cm^{-1} mM^{-1} between oxidized and reduced enzyme, the amplitude change for this phase accounts for the reduction of approximately 80% of input enzyme, including the reaction that occurred during the mixing dead time. From these data it is clear that the DHO binding step occurs during the mixing dead time. The second kinetic phase displayed no clear dependence upon DHO concentration and $k_{2,red}$ ranged from 8 to 15 s^{-1} for the wild-type enzyme (Table 3-2 and Figure 3-5). These experiments were repeated for the mutant enzymes and similar results to the wild-type enzyme were obtained (Table 3-2). Thus, mutation of residues in the A77 1726 binding-site has no significant effect on the reductive half-reaction catalyzed by *Pf* DHODH.

I have assigned the first observed kinetic step ($k_{1,red}$) as the rate of the chemical step in which FMN is reduced and DHO is oxidized (Scheme 3-2). The second step could reflect several processes such as orotate release or a conformational change associated with its release, however, without additional data it is not possible to fully assign this step. Given the fact that these data were collected at a lower temperature than the steady-state data (4°C vs 25 ^{o}C), at equivalent temperatures both $k_{1,red}$ and $k_{2,red}$ would be faster than the steady-state rate (Tables 1 and 2).

Pre-steady-state Kinetic Analysis of the FMN Oxidative Half-reaction

The oxidative half-reaction was also examined by single wavelength stopped-flow spectroscopy. Oxidized wild-type enzyme (45 μM) was reduced in anaerobic buffer by the addition of a limiting amount of DHO (30 μM) under an atmosphere of nitrogen before loading onto the stopped-flow instrument. Reduced enzyme (10 μM) was then mixed with CoQ_1 (31–500 μM), final concentrations. FMN oxidation was observed at 485 nm at 4°C over a time range of 4–500 ms (approximately ten half-lives of the slowest rate) and the resulting data were fitted to Equation 3-2. The data were well fit by a single exponential (Figure 3-6). This kinetic phase was dependent on CoQ_1 concentration and the k_{obs} data for the wild-type enzyme were fitted to Equation 3-3 ($K_{d,ox}$ = 67 ± 5 μM; k_{ox} = 67 ± 2 s^{-1}). The CoQ binding step occurred during the mixing dead time. The absorbance change of this phase suggests it reflects the chemical step for the conversion of FMN from the reduced to the oxidized state (Scheme 3-3). This rate at 4°C is 6-fold faster than the steady-state rate at 25°C, suggesting this chemical step is not rate-limiting for the entire reaction cycle.

Analysis of the oxidative half-reaction by stopped-flow spectroscopy was undertaken for six of the A77 1726 binding-site mutant enzymes (H185A, F188A, F227A, R265A, I272A, and Y528A). The mixing protocol and data collection were performed identically to the wild-type enzyme (as above). The data were best fitted to Equation 3-2 using a single exponential, and the resulting k_{obs} values were fitted to Equation 3-3 to determine the kinetic constants for the reaction

(Table 3-2). The mutant enzymes tested exhibit a range of k_{ox} values, with H185A and Y528A displaying an approximate 20-fold decrease in catalytic rate compared to wild-type enzyme. Mutation to alanine of F188, F227, and R265 result in a 2–9-fold decrease in catalytic rate. In contrast, the mutant enzymes display little variation in $K_{d,ox}$ for CoQ_1 compared to wild-type enzyme. Mutation of the two charged residues within the A77 1726 binding-site, H185 and R265, actually result in a two- to four-fold decrease, respectively, in K_d for CoQ_1, implying slightly tighter substrate binding to these mutant enzymes. These data show mutation of residues in the A77 1726 binding-site affect the rate of the CoQ dependent flavin oxidative half-reaction, but have little affect on the binding affinity of CoQ to the enzyme.

Effect of A77 1726 Binding Site Inhibitors on the Pf DHODH Oxidative and Reductive Half-reactions

Previously, we identified DCPMNB as a potent and species selective inhibitor of the malarial enzyme. DCPMNB showed competitive inhibition toward ubiquinone analogue substrates [35]. Further, the effect of the H185A and R265A mutants on the binding of this inhibitor was characterized, leading to the conclusion that it bound to the A77 1726 binding-site. To extend these data, I characterized the effect of the additional A77 1726 binding-site mutations on DCPMNB inhibition. DCPMNB inhibits the steady-state reaction in the presence of CoQ_1 or CoQ_D (100 μM) with an IC_{50} of 50 and 70 nM, respectively (Figure 3-

7), while A77 1726 is a relatively weak inhibitor of *Pf* DHODH (IC_{50} = 180 ± 3 μM). The IC_{50} for DCPMNB was substantially increased (40–240-fold) by three of the five tested mutations, confirming our prior conclusion that it binds to the A77 1726 site (Table 3-3). I also examined the ability of DCPMNB to inhibit wild-type *Pf* DHODH steady-state kinetics when the terminal electron acceptor is molecular oxygen or ferricyanide. Interestingly, in the presence of these inorganic oxidants, little inhibition was observed even at the highest concentration of DCPMNB tested (100 μM). These results demonstrate lack of inhibition by DCPMNB when the steady-state reaction progresses in the presence of inorganic electron acceptors ferricyanide or oxygen, and shows that this inhibitor specifically blocks electron transfer to ubiquinone analogues.

The effect of A77 1726 and DCPMNB on the oxidative and reductive *Pf* DHODH half-reactions was examined under saturating concentrations of each inhibitor using the rapid mixing protocols described above. For the DHO-dependent reductive half-reaction, neither inhibitor had a significant effect on the reaction, while orotic acid, the product of the reductive half-reaction, fully inhibited the reaction (Figure 3-8). In contrast, when the CoQ_1-dependent oxidative half-reaction was examined, the reaction was fully inhibited in by both A77 1726 and DCPMNB (Figure 3-9), indicating that these inhibitors specifically block the CoQ_1-dependent oxidative half-reaction.

CONCLUSIONS

DHODH is an important drug target for the treatment of human rheumatoid arthritis, and a growing body of literature suggests that targeting the enzyme from the human malarial parasite may provide new chemotherapeutic approaches for this devastating human infection. Identified inhibitors (e.g. A77 1726) of both the human and parasite enzyme bind to a pocket adjacent to the FMN cofactor but on the opposite face from the DHO binding site [27, 34]. While the prevailing hypothesis has been that the physiological oxidant CoQ also binds this site, the available experimental evidence has not fully supported this hypothesis [51]. In order to provide insight into the CoQ binding-site and the mechanism of both catalysis and inhibition, I characterized a series of A77 1726 binding-site mutations. The data revealed that none of the mutations caused a substantial change in the reductive half-reaction, but instead affect the rate of the oxidative half-reaction without substantially affecting the dissociation constant for CoQ_1. Overall, the mutations affected the rates of the steady-state reaction, the oxidative half-reaction, or both, but none had measurable affects on the binding steps of these processes. In contrast, the mutations did cause substantial increases in the IC_{50} values for A77 1726 binding-site inhibitors. Further, A77 1726 and a *Pf* DHODH specific inhibitor (DCPMNB) block the oxidative half-reaction, but not the reductive half-reaction. The data suggest the binding sites for CoQ and A77 1726 site inhibitors are not directly overlapping, and they support an alternative model whereby instead of directly competing with CoQ, inhibitors

disrupt the electron flow between FMN and CoQ bound to a more distal, but as of yet unidentified site.

Comparison of the steady-state and pre-steady state data provides insight into the rate-limiting step for the reaction catalyzed by *Pf* DHODH. For the wild-type enzyme, the reductive half-reaction was characterized by two observable kinetic steps. The first of these ($k_{1,red}$) was substantially faster than the steady-state rate even though the steady-state data were collected at a higher temperature (25°c vs 4°C). This step reflects the chemical reduction of FMN, and suggests that the rate of FMN reduction/DHO oxidation is substantially faster than the rate-determining step. This reductive half-reaction rate is comparable to that found for the Family 2 human and *E. coli* DHODH enzymes [41, 42]. The second observed phase ($k_{2,red}$) was significantly slower in rate, but given the temperature difference in the experimental conditions this rate is also estimated to be 3–4-fold higher than the steady-state rate. It is possible that this step reflects orotic acid release, but it may also reflect a conformational change or other undefined step along the reaction coordinate. Similarly, the single observable kinetic step for the oxidative half reaction was substantially faster than the steady-state rate, and thus demonstrates that oxidation of FMN by CoQ is not rate-determining for the reaction cycle. The CoQ-dependent rate for the *P. falciparum* enzyme is 3–5-fold slower than the menadione-dependent oxidative half-reaction rate determined for

the *E. coli* enzyme [42]. I have no data that reflects on the rate of CoQ product release, and this step could in turn limit the overall reaction rate.

The finding that A77 1726 binding-site mutations affected the rate of the oxidative but not the reductive half-reaction catalyzed by *Pf* DHODH suggests that these residues are involved in electron transfer between FMN and CoQ. For H185A and Y528A, k_{ox} was decreased approximately 25-fold, while mutation of F188, F227, or R265 to Ala produces a 2–9-fold decrease in catalytic rate. As mutation of Y528 also causes a 4-fold decrease in the steady-state reaction when oxygen is used as a co-substrate, these data suggest a general effect on the rate of electron transfer to acceptor substrates for this residue. Aromatic substitution of Y528 by phenylalanine or tryptophan partially restores the steady-state reaction for all electron acceptors, suggesting either the aromaticity or planarity of the side-chain, which stacks against the FMN cofactor, is important for electron transfer. Y528 is completely conserved in Family 2 DHODH enzymes. Involvement of Y528 in either electron transfer or proton donation after electron transfer to ubiquinone substrates has been suggested [18, 27], and my data support those hypotheses. The steady-state and rapid kinetics data presented here further suggest that a number of residues in the A77 1726 binding-site play roles in the electron transfer step between FMN and CoQ, though they do not identify a specific electron transfer pathway.

Finally, my analysis of the A77 1726 binding site mutants suggests that CoQ does not share this binding site. Previous studies found that inhibitors which bind the A77 1726 binding site (e.g. brequinar, DCPMNB) were competitive inhibitors of CoQ substrates [35, 50, 51]. However, the mutations in the A77 1726 binding site do not have significant effects on the K_m for the steady-state reaction nor on the DHO- or CoQ-dependent K_d's observed for the reductive or oxidative half-reactions, respectively. In contrast, mutation of H185, F188, or F227 causes a large increase (60-, 40-, and 245-fold, respectively) in the IC_{50} for DCPMNB, consistent with the hypothesis that this inhibitor binds the A77 1726 binding-site. While these data do not support a model where CoQ shares an overlapping binding site with A77 1726, my data do show that both A77 1726 and DCPMNB are able to specifically block electron transfer between FMN and CoQ, as these inhibitors block only the oxidative half-reaction. Further, these inhibitors are unable to block FMN oxidation by non-specific inorganic oxidants (O_2 or ferricyanide), which presumably are able to utilize alternative electron paths for FMN oxidation. These results suggest that electron transfer from FMN occurs through one or more of the A77 1726 binding site residues to a more distant ubiquinone binding site, possibly closer to the surface of the protein at the enzyme-membrane interface. Inhibitors of the CoQ-dependent reaction could act by either obstructing the binding of those co-substrates at a distant but non-overlapping binding site, or by preventing the electron transfer to those co-

substrates. Under such a model, CoQ would block inhibitor binding into the channel (e.g. by blocking the channel entrance) while inhibitors would disrupt the electron transfer path between CoQ and FMN. This model would also yield competitive inhibition kinetics despite the possibility that CoQ and inhibitor do not bind to overlapping sites.

The N-terminus of both human and *Pf* DHODH is composed of outward-facing hydrophobic residues, which have been implicated in the partial burial ubiquinone binding site into the mitochondrial membrane [27, 34, 78, 79]. This arrangement may allow natural and synthetic ubiquinone substrates to be positioned near the surface of the N-terminal domain, rather than deep within the A77 1726 inhibitor binding channel formed by the two N-terminal helices. Electrons could readily be channeled or tunneled from FMN to a distantly bound ubiquinone at the membrane surface through one or more of the residues within the A77 1726 binding site. Electron transfer by tunneling through the protein backbone or the protein medium has been described for respiratory and photosynthetic enzymes, as has long distance hydrogen transfer [80-82]. Additionally, long range electron transfer from FMN to a distant electron acceptor has been discussed previously for the *E coli* enzyme [42]. Defining the exact route(s) of electron transfer would be greatly supported by a co-crystallized enzyme/CoQ substrate structure model.

EQUATIONS

$$v_i = \frac{v_o}{1 + \frac{[\mathrm{I}]}{\mathrm{IC}_{50}}}$$

Equation 3-1 IC_{50} equation.

$$A = \sum_{i=1}^{n} A_i e^{-k_{obs} i t} + b$$

Equation 3-2 Exponential equation.

$$k_{obs} = \frac{k_1[\mathrm{S}]}{K_m + [\mathrm{S}]}$$

Equation 3-3 Henri-Michaelis-Menten equation.

SCHEMES

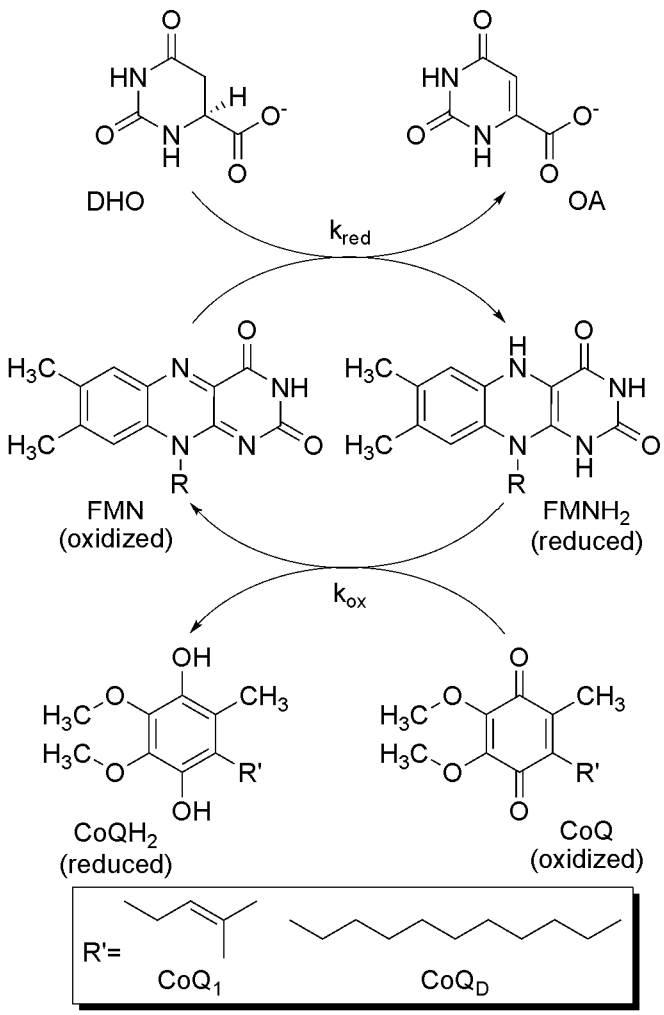

Scheme 3-1 DHODH reaction.

$$E_{ox} + DHO \underset{}{\overset{K_{d,red}}{\rightleftharpoons}} E_{ox}\text{-}DHO \underset{\text{(fast)}}{\overset{k_{1,red}}{\rightleftharpoons}} E_{red}\text{-}OA \underset{\text{(slow)}}{\overset{k_{2,red}}{\rightleftharpoons}} E_{red}\sim OA$$

Scheme 3-2 Reductive half-reaction.

$$E_{red} + CoQ \overset{K_{d,ox}}{\rightleftharpoons} E_{red}\text{-}CoQ \overset{k_{ox}}{\rightleftharpoons} E_{ox}\text{-}CoQH_2$$

Scheme 3-3 Oxidative half-reaction.

TABLES

	O_2	Q_1		Q_D	
Pf DHODH	k_{cat} (s^{-1})	K_m^{app} (μM)	k_{cat} (s^{-1})	K_m^{app} (μM)	k_{cat} (s^{-1})
wt	0.42 ± 0.01	11 ± 2	7.8 ± 0.3	13 ± 1	12 ± 1
H185A	0.57 ± 0.04	22 ± 3	7.3 ± 2.2	34 ± 9	7.9 ± 3.3
F188A	0.53 ± 0.03	15 ± 3	2.6 ± 0.4	20 ± 3	4.3 ± 0.2
F227A	0.43 ± 0.05	16 ± 2	2.6 ± 0.1	20 ± 3	3.5 ± 0.2
R265A	0.44 ± 0.02	38 ± 3	3.1 ± 0.1	26 ± 1	5.0 ± 0.1
I272A	0.083 ± 0.004	7.8 ± 0.4	1.5 ± 0.1	12 ± 1	1.8 ± 0.1
Y528A	0.10 ± 0.01	16 ± 3	0.19 ± 0.03	8.8 ± 2.3	0.12 ± 0.01
Y528F	0.63 ± 0.03	20 ± 3	1.9 ± 0.1	53 ± 4	1.2 ± 0.1
Y528W	0.18 ± 0.01	48 ± 14	5.1 ± 0.6	45 ± 11	6.8 ± 0.7
L531A	0.25 ± 0.02	17 ± 2	5.1 ± 0.9	16 ± 1	8.6 ± 1.4

Table 3-1 Steady-state kinetic parameters of wild-type and mutant *Pf* DHODH. Steady-state experiments were performed at 25°C. Values for k_{cat} and K_M^{app} for a variety of electron acceptors were derived as described in the text.

	reductive half-reaction			oxidative half-reaction	
Pf DHODH	$K_{d,red}$ (μM)	$k_{1,red}$ (s^{-1})	$k_{2,red}$ (s^{-1})	$K_{d,ox}$ (μM)	k_{ox} (s^{-1})
wt	230 ± 70	350 ± 30	8.2 ± 0.4	67 ± 5	67 ± 2
H185A	98 ± 42	180 ± 10	9.9 ± 1.6	32 ± 3	2.8 ± 0.1
F188A	100 ± 20	180 ± 10	5.7 ± 0.5	74 ± 3	16 ± 1
F227A	120 ± 10	180 ± 10	6.2 ± 0.6	90 ± 9	26 ± 1
R265A	78 ± 8	200 ± 10	8.0 ± 0.7	14 ± 1	7.4 ± 0.1
I272A	94 ± 28	210 ± 20	6.4 ± 0.7	87 ± 6	77 ± 2
Y528A	70 ± 29	200 ± 10	8.7 ± 0.7	51 ± 5	2.9 ± 0.1
L531A	150 ± 10	300 ± 10	7.4 ± 1.2	nd	nd

Table 3-2 Pre-steady-state burst phase rates of wild-type and mutant *Pf* DHODH. Pre-steady-state experiments were performed at 4°C. Values for K_d and $k_{red/ox}$ were derived as described in the text.

Pf DHODH	DCPMNB IC_{50} (nM)
wt	49 ± 1
H185A	2900 ± 100
F188A	1900 ± 100
F227A	12000 ± 1000
R265A	100 ± 10
L531A	87 ± 1

Table 3-3 IC_{50} values for *Pf* DHODH inhibition by DCPMNB. Inhibition was examined in the presence of 500 μM DHO and 20 μM CoQ_D using 5 nM enzyme.

FIGURES

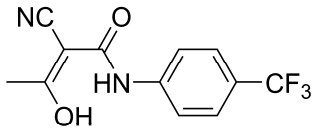

A77 1726

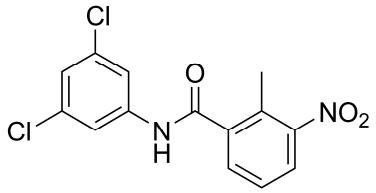

DCPMNB

Figure 3-1 DHODH inhibitors.

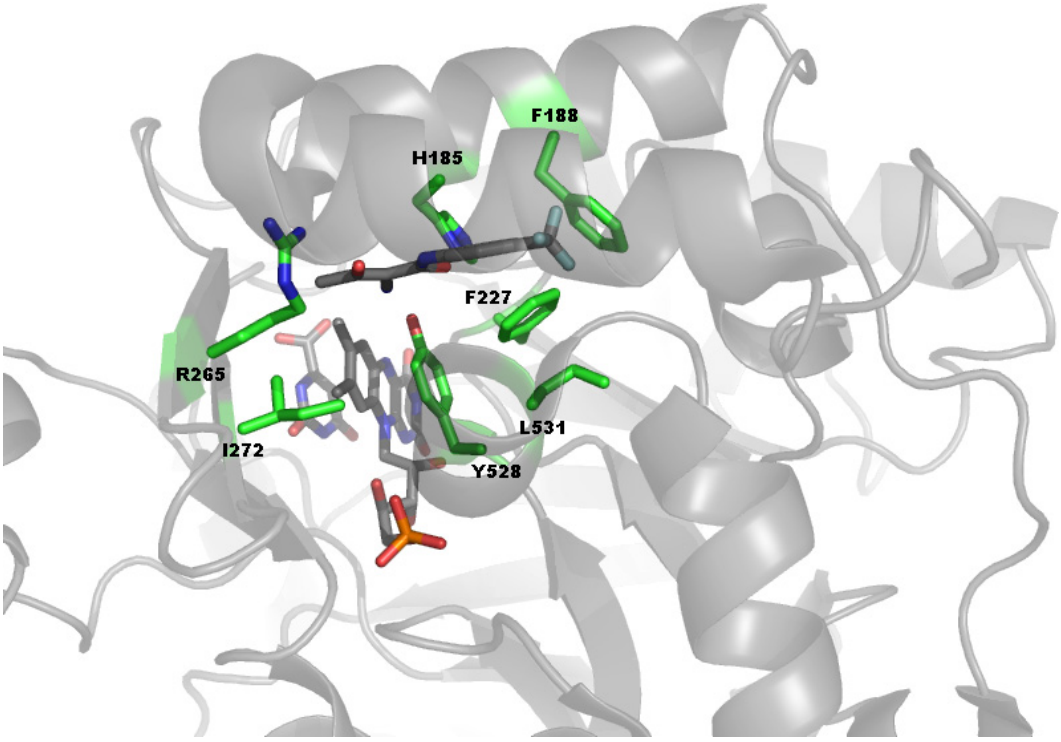

Figure 3-2 Inhibitor binding site of *Pf* DHODH. A cartoon drawing of the enzyme backbone is colored gray. Oxygen is colored red, nitrogen blue, fluorine cyan, carbon atoms of inhibitor A77 1726, FMN, and product orotate are colored gray, carbon atoms of residues within 4 Å of the inhibitor chosen for mutation are displayed and colored green. Residue F188 is an alanine and residue I272 is a valine in the human enzyme. All other residues displayed are conserved between the two species.

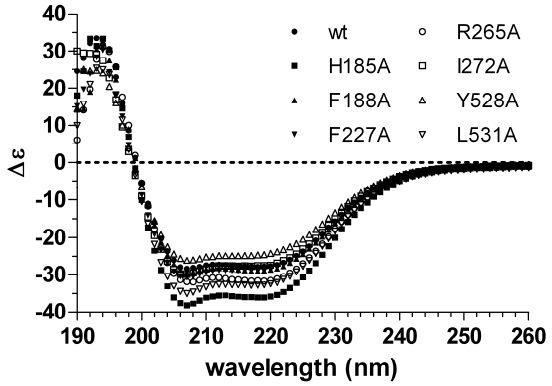

Figure 3-3 Circular dichroism spectroscopic analysis of wild-type and mutant *Pf* DHODH. Spectra were obtained from 8 μM protein samples in a 1 mm path length cuvette.

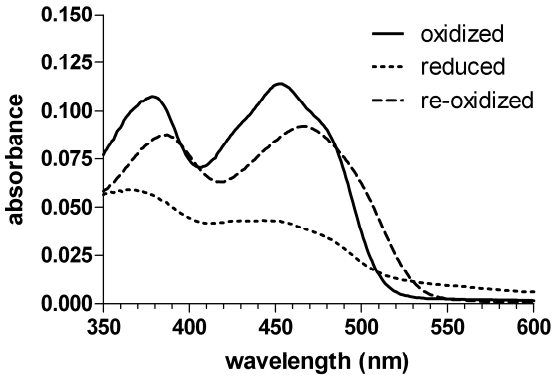

Figure 3-4 Absorbance spectra of wild-type *Pf* DHODH. The 10 μM enzyme sample is oxidized (solid line) in buffer containing dissolved oxygen. The enzyme sample was reduced (dotted line) by the addition of 500 μM DHO and the absorbance spectrum was recorded immediately. The reaction with DHO and dissolved oxygen was allowed to proceed for several minutes to completion and the absorbance spectrum of re-oxidized enzyme, now in the presence of product orotate, was recorded (dashed line).

a)

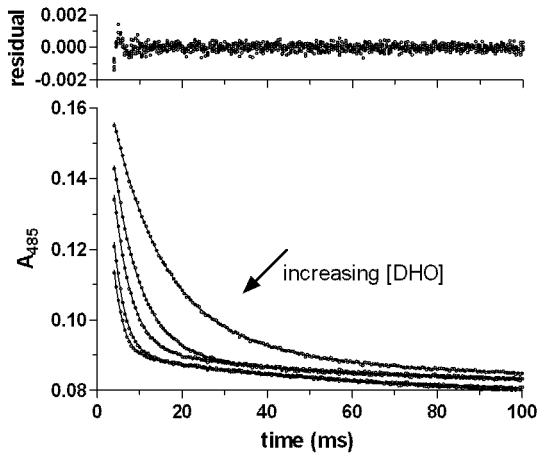

b)

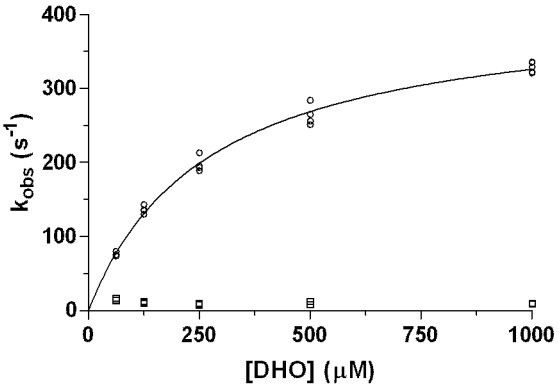

Figure 3-5 Pre-steady-state burst kinetics of wild-type *Pf* DHODH reductive half-reaction. (a) Absorbance traces (closed circles) for *Pf* DHODH (final concentration 20 μM) after rapid mixing with DHO (final concentrations 62, 125, 250, 500, 1000 μM) at 4°C. Data were fitted to Equation 3-2 using double exponentials (solid curves) to obtain k_{obs} values. The residual plot for the fit are displayed above the graph. (b) The DHO concentration dependence of $k_{obs,1}$ and $k_{obs,2}$ (open circles and open squares, respectively). The $k_{obs,1}$ for the first observed kinetic step was fitted to Equation 3-3 ($K_{d,red}$ = 230 ± 70 μM; $k_{1,red}$ = 350 ± 30 s^{-1}).

a)

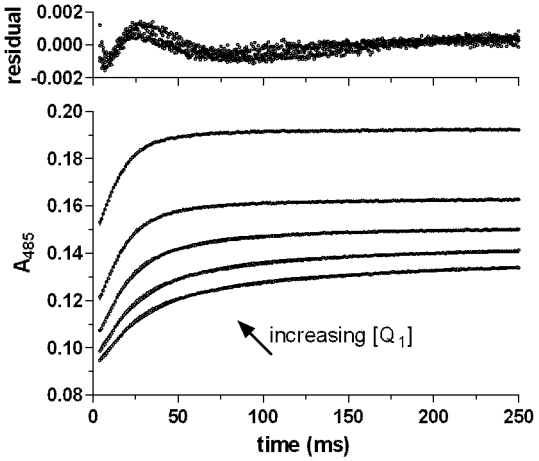

b)

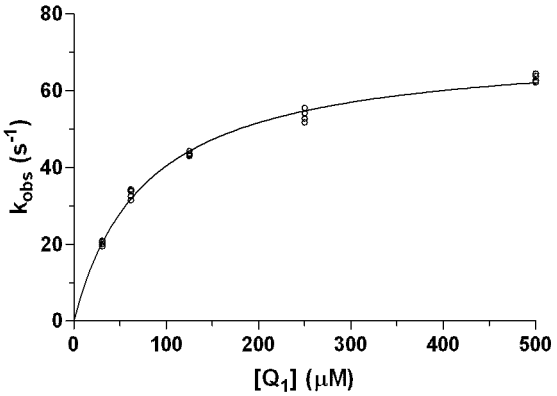

Figure 3-6 Pre-steady-state burst kinetics of wild-type *Pf* DHODH oxidative half-reaction. (a) Absorbance traces (closed circles) are displayed for enzyme (15 μM enzyme pre-reduced with 10 μM DHO, final concentrations) after rapid mixing with CoQ_1 (final concentrations 31, 62, 125, 250, 500 μM) at 4°C. Data were fitted to Equation 3-2 using a single exponential (solid curve). The residual plot for the fit are displayed above the graph. (b) CoQ_1 concentration dependence of the k_{obs} (open circles). The k_{obs} for the observed kinetic step was fitted to the Equation 3-3 to determine the kinetic parameters ($K_{d,ox} = 67 \pm 5$ μM; $k_{ox} = 67 \pm 2$ s^{-1}).

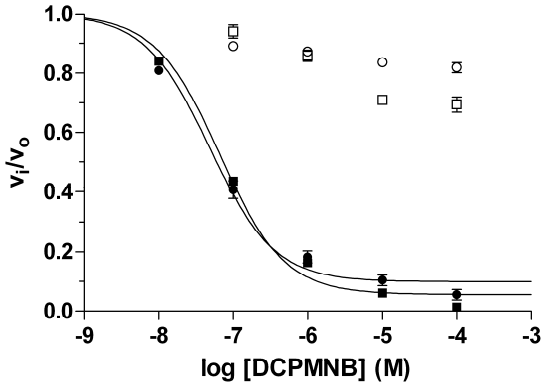

Figure 3-7 Inhibition of wild-type *Pf* DHODH steady-state reaction by DCPMNB using different electron acceptors. The steady-state reaction was allowed to proceed in the presence of dissolved oxygen (~300 μM) (open circles) or 100 μM $K_3Fe(CN)_6$ (open squares), CoQ_1 (closed circles), or CoQ_D (closed squares). Data for CoQ_1 and CoQ_D produce an IC_{50} of 48 and 66 nM, respectively. Inhibition at 100 μM DCPMNB is 12% and 30% for oxygen- and $K_3Fe(CN)_6$-dependent activity and could not be fit to an IC_{50} equation.

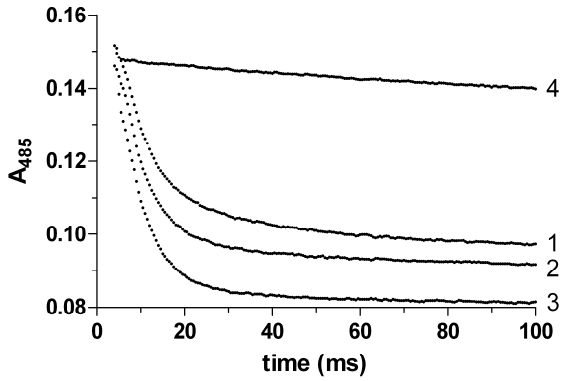

Figure 3-8 Pre-steady-state burst kinetics of wild-type *Pf* DHODH in the presence of inhibitors (reductive half-reaction). Absorbance traces of 20 μM enzyme alone (trace 1) or pre-mixed with 50 μM DCPMNB (trace 2), 1 mM A77 1726 (trace 3), or 1 mM OA (trace 4) and then mixed with 125 μM DHO. All concentrations are after mixing.

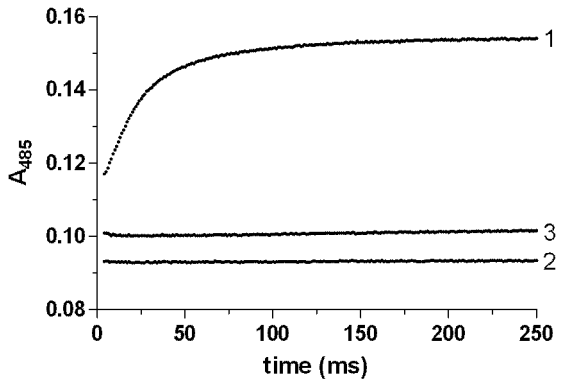

Figure 3-9 Pre-steady-state burst kinetics of wild-type *Pf* DHODH in the presence of inhibitors (oxidative half-reaction). Absorbance traces of enzyme (15 μM pre-reduced with 10 μM DHO) alone (trace 1) or pre-mixed with DCPMNB (50 μM) (trace 2) or A77 1726 (1 mM) (trace 3) and then mixed with CoQ_1 (100 μM). All concentrations are after mixing.

CHAPTER FOUR
Further Analysis

INTRODUCTION

There are some additional experiments which were not compiled into manuscripts, as the data from the previous two chapters were, but nonetheless bear mentioning. These studies are necessarily "miscellaneous," and represent both preliminary and follow-up work. I will also discuss some experiments which did not produce any publishable data; however, the overall findings of this dissertation provide an explanation as to why those experiments were unsuccessful.

EXPERIMENTAL PROCEDURES

Methods

Enzyme kinetic assays

All *Pf* DHODH enzyme assays described in this chapter were performed similarly to those described elsewhere in this work. Any deviations are described below.

Product inhibition was examined using a range of co-substrate and orotate concentrations. The concentration of CoQ_D was held at 100 μM when observing DHO-dependent inhibition; the concentration of DHO was held at 500 μM when CoQ_D-dependent inhibition was examined. These assays were performed in the presence of 0.1% Triton X-100 in the enzyme assay buffer described previously.

Observation of the effect of pH on enzyme activity utilized a buffer system originally developed for crystallography screens [83]. The buffer system is composed of succinic acid, monobasic sodium phosphate, and glycine in a 2:7:7 ratio. The total molarity of the system is 100 mM such that it contains 12 mM succinate, 44 mM phosphate, and 44 mM glycine. Two individual 1 molar buffer stocks are made at pH 4.0 and 10.0. Subsequent buffers at different intermediate pH values are made from mixtures of these two stock buffers. This buffer also contains 150 mM NaCl, 10% glycerol, and 0.1% Triton X-100. Oxidase activity was observed in the presence of 500 μM DHO and no additional CoQ co-substrate. CoQ_D activity was observed in the presence of 500 μM DHO and 100 μM CoQ_D.

Surface dilution kinetic analyses of *Pf* DHODH mutants were performed exactly as for wild-type enzyme.

RESULTS

Ping-pong Kinetics

A steady-state analysis of the bi-reactant *Pf* DHODH kinetic mechanism was attempted to confirm that the enzyme performs catalysis similar to other DHODH enzymes [39, 43, 84]. The initial velocity pattern of *Pf* DHODH catalysis across a range of DHO and CoQ_D co-substrate concentrations displayed parallel lines consistent with a ping-pong kinetic model (Figure 4-1).

Product Inhibition by Orotate

The *Pf* DHODH reaction was investigated for product inhibition by orotate (Figure 4-2). Orotate was examined as an inhibitor of both the DHO-dependent reaction and the CoQ_D-dependent reaction. The data show very clearly that orotate is a competitive inhibitor toward DHO and an uncompetitive inhibitor toward CoQ_D. The resulting inhibition constants are $K_i = 27 \pm 3$ μM for DHO and $\alpha K_i = 44 \pm 2$ μM for CoQ_D.

Effect of pH on Wild-type and Mutant Pf DHODH Catalysis

The pH-dependent activity of wild-type and mutant *Pf* DHODH was examined to potentially identify ionizable residues involved in substrate binding or catalysis of oxygen and ubiquinone substrates. Mutants of ionizable residues included H185A, R265A, C276A, and the aromatic replacement mutants Y528F and Y528W. Oxidase activity for wild-type and mutant *Pf* DHODH is essentially the same, displaying an increase in activity with increasing pH (Figure 4-3). Wild-type CoQ_D-dependent activity indicates the presence of two ionizable residues with pK values of 6.1 and 8.6 (Figure 4-4). One of these pKa values represents the DHO active-site serine while the other may reflect an ionizable residue responsible for ubiquinone substrate binding or catalysis. Mutation of ionizable residues in the A77 1726 site results in alterations of the wild-type pH activity profile (Figure 4-4). The C278A mutant shifts the peak of activity one pH-unit higher, while the H185A and Y528F mutants broaden the pH-dependent activity profile relative to wild-type enzyme. However, the complete loss of one ionizable

group is not apparent for any mutant, suggesting none of these residues is solely responsible for one arm of the wild-type pH profile.

Surface Dilution Kinetic Analysis of Pf DHODH Mutants

Surface dilution kinetic analysis of the wild-type enzyme produced values for the apparent dissociation constant for the mixed micelle binding site (K_s^A) and the apparent interfacial Michaelis constant (K_m^B). Though no substantial differences in the K_M^{app} for ubiquinone analogues were revealed by steady-state kinetic analysis of the A77 1726 binding site mutants, it remained possible that alterations in substrate affinity could be uncovered by surface dilution kinetic analysis. The mutants H185A, F188A, F227A, R265A, and Y528W were therefore subjected to surface dilution kinetic analysis using CoQ_D in Tween-80 micelles (Table 4-1). The results mirror those of the standard steady-state kinetic analysis, i.e., variations in catalytic rate but no significant alteration in the two apparent affinity terms. These findings show that even a more thorough examination of CoQ utilization by these mutants using surface dilution kinetic analysis does not reveal any differences in catalysis other than catalytic rate term.

DISCUSSION

These several experiments offer some insight into the *Pf* DHODH catalytic mechanism. The observation of ping-pong kinetics confirms this enzyme operates similarly to other DHODH enzymes studies thus far [39, 43, 84]. The examination of product inhibition by orotate served two purposes. First, the

experiment establishes that product inhibition does indeed occur for this enzyme. Second, the data indicate orotate is competitive toward the DHO-dependent reaction and uncompetitive toward the CoQ_D-dependent reaction. CoQ_D-dependent orotate inhibition by either a non-competitive or an uncompetitive mode signifies either a random or a sequential two site ping-pong model, respectively. These results, combined with the observation of ping-pong kinetics, support a sequential two-site kinetic model for *Pf* DHODH. The bovine liver DHODH enzyme was found to display a "rapid equilibrium random (two-site) hybrid ping-pong reaction" where an inhibitor of the DHO-dependent reaction is competitive with DHO and either non-competitive or uncompetitive with CoQ [43].

The pH dependence of oxygen and CoQ_D catalysis was undertaken in an attempt to identify ionizable residues responsible for that half-reaction. The data indicate these mutations affect oxidase activity to a minimal extent. Though differences in pH profile are observed across wild-type and mutant *Pf* DHODH, the resulting profiles do not clearly indicate any of these ionizable residues are solely responsible for one of the pKa values. Had mutation of one of the residues abolished one arm of the pH profile, the follow-up experiment would be to examine the pH-dependent K_M^{app} or k_{cat} of that mutant compared to wild-type enzyme, which would indicate the residue is involved in CoQ binding or catalysis, respecitvely.

Surface dilution kinetic analysis of *Pf* DHODH mutants was performed to determine if mutation results in a substantial change in the K_s^A or K_m^B parameters. As these terms separate initial association of the enzyme with the substrate from subsequent catalytic steps, it remained possible that mutation would cause a significant change in one or the other surface dilution kinetic terms that would not be revealed in simple steady-state kinetic analysis. However, only alterations in the V_{max} term were uncovered, similar to the simple steady-state analysis. These results suggest that the effect of mutation is only on catalytic rate.

The initial goal of this project was to identify residues responsible for ubiquinone co-substrate binding and catalysis. Steady-state kinetic experiments in combination with alanine mutagenesis were performed to identify residues which alter the kinetic parameters of ubiquinone co-substrate-dependent catalysis. Specifically, an increase in K_M^{app} upon mutation would have revealed residues involved in co-substrate binding. The results of these experiments, however, showed alterations in k_{cat} upon mutation of several residues, but no significant changes in K_M^{app}. This prompted the search for a ubiquinone binding assay.

The first binding assay was based upon the FMN spectral shift produced when a planar ligand stacks against tightly-bound FMN. This type of experiment has been successful in determining a dissociation constant for orotate for some DHODH enzymes [36, 84, 85]. Numerous attempts at a similar binding assay using a variety of ubiquinone co-substrate analogues (CoQ_0, CoQ_1, CoQ_D) were

unsuccessful, as were analogous experiments based upon tryptophan fluorescence of the Y528W mutant. In retrospect, ubiquinone co-substrate analogues bind at least on the other side of the Y528 residue, and likely much farther out of the proposed ubiquinone binding site. These experiments, therefore, would not have produced the effect on FMN absorbance or fluorescence that is seen with orotate binding.

The second assay utilized isothermal titration calorimetry to examine both orotate and CoQ_0 binding from a thermodynamic point of view. The results from these experiments were difficult to interpret clearly. Control experiments designed to observe orotate binding would often produce binding curves indicative of a dissociation constant similar to the K_M for DHO, but would suggest an enzyme-to-orotate stochiometry of 2:1. Other experiments would produce data that fit best to a two-site model with different dissociation constants, or would reveal very little heat of interaction and therefore not fit any binding model. Experiments using CoQ_0 were similarly inconsistent, and when data would fit a binding model the enzyme-to-CoQ_0 stochiometry would often be near 1:3.

The difficulty with these experiments can be explained by a variety of detergent effects. Isothermal titration calorimetry reports on any process that involves a change in heat. Several results within this dissertation show that substrate partitioning into detergent micelles can be observed by isothermal titration calorimetry. Also, *Pf* DHODH does aggregate under certain conditions as

a function of detergent type and concentration, a process which is likely to elicit or absorb some heat measurable in the calorimeter. These general effects could explain some of the inconsistencies associated with this method. Ultimately, however, the rapid kinetic analysis of the oxidative half-reaction, which revealed little change in K_d for CoQ_1 suggest that none of the residues tested would have shown a difference in substrate binding given a robust binding assay.

TABLES

	V_{max} (s^{-1})	K_s^A (μM)	K_m^B (mol%)
wt	7.4 ± 0.3	7.0 ± 1.8	0.32 ± 0.07
H185A	2.8 ± 0.2	9.0 ± 1.4	0.76 ± 0.12
F188A	1.3 ± 0.1	6.3 ± 2.5	0.27 ± 0.08
F227A	1.3 ± 0.1	6.1 ± 1.7	0.32 ± 0.08
R265A	4.7 ± 0.4	9.2 ± 3.0	0.49 ± 0.14
Y528W	2.9 ± 0.2	6.6 ± 2.1	0.59 ± 0.16

Table 4-1 Surface dilution kinetic values for wild-type and mutant *Pf* DHODH. V_{max} is the extrapolated V_{max} at infinite substrate concentration and unity mole fraction of CoQ substrate, K_s^A is the apparent dissociation constant for the mixed micelle binding site under the "substrate binding model", and K_m^B is the apparent interfacial Michaelis constant.

FIGURES

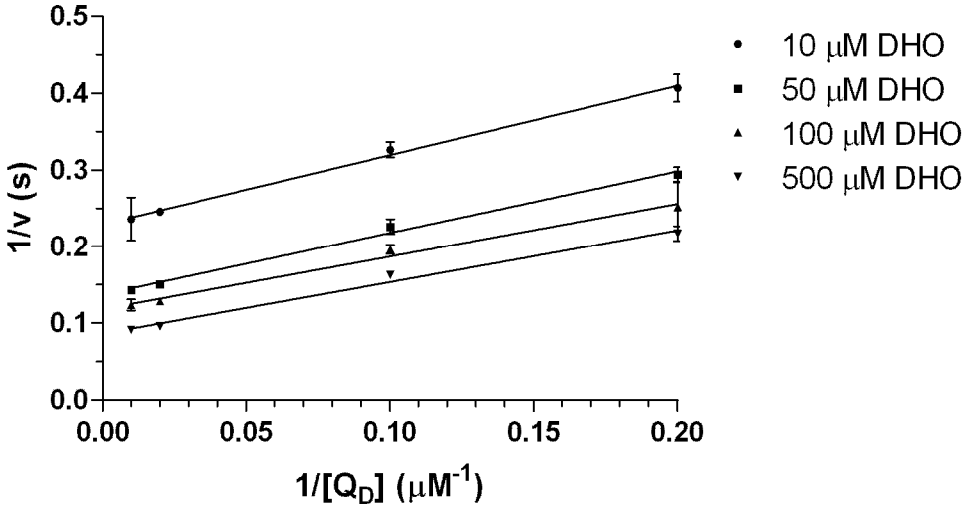

Figure 4-1 Ping-pong kinetics of *Pf* DHODH. Double reciprocal plot of CoQ_D-dependent activity at several concentrations of DHO. The slopes of the lines through the data are not statistically different.

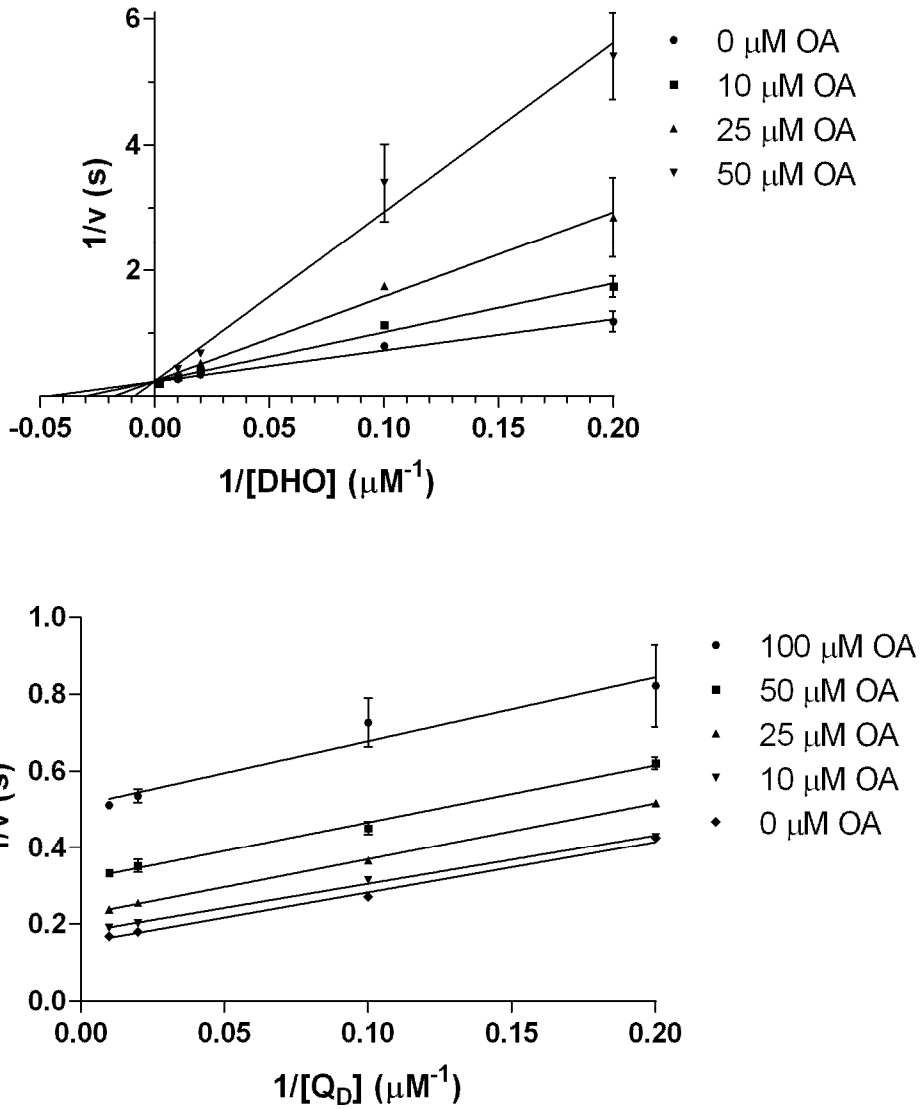

Figure 4-2 Orotate acid inhibition of DHO- and CoQ_D-dependent *Pf* DHODH activity. Double reciprocal plots of DHO- (top) and CoQ_D-dependent (bottom) activity in the presence of several orotate concentrations. The fitted lines for the DHO-dependent reaction cross the 1/v axis at essentially the same point; those for the CoQ_D-dependent reaction have essentially the same slope.

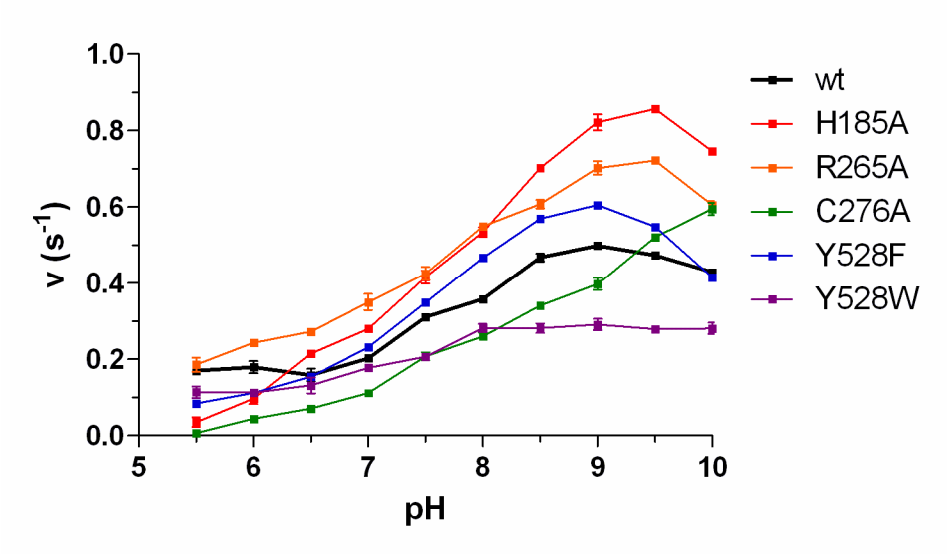

Figure 4-3 pH-dependent oxidase activity of wild-type and mutant *Pf* DHODH.

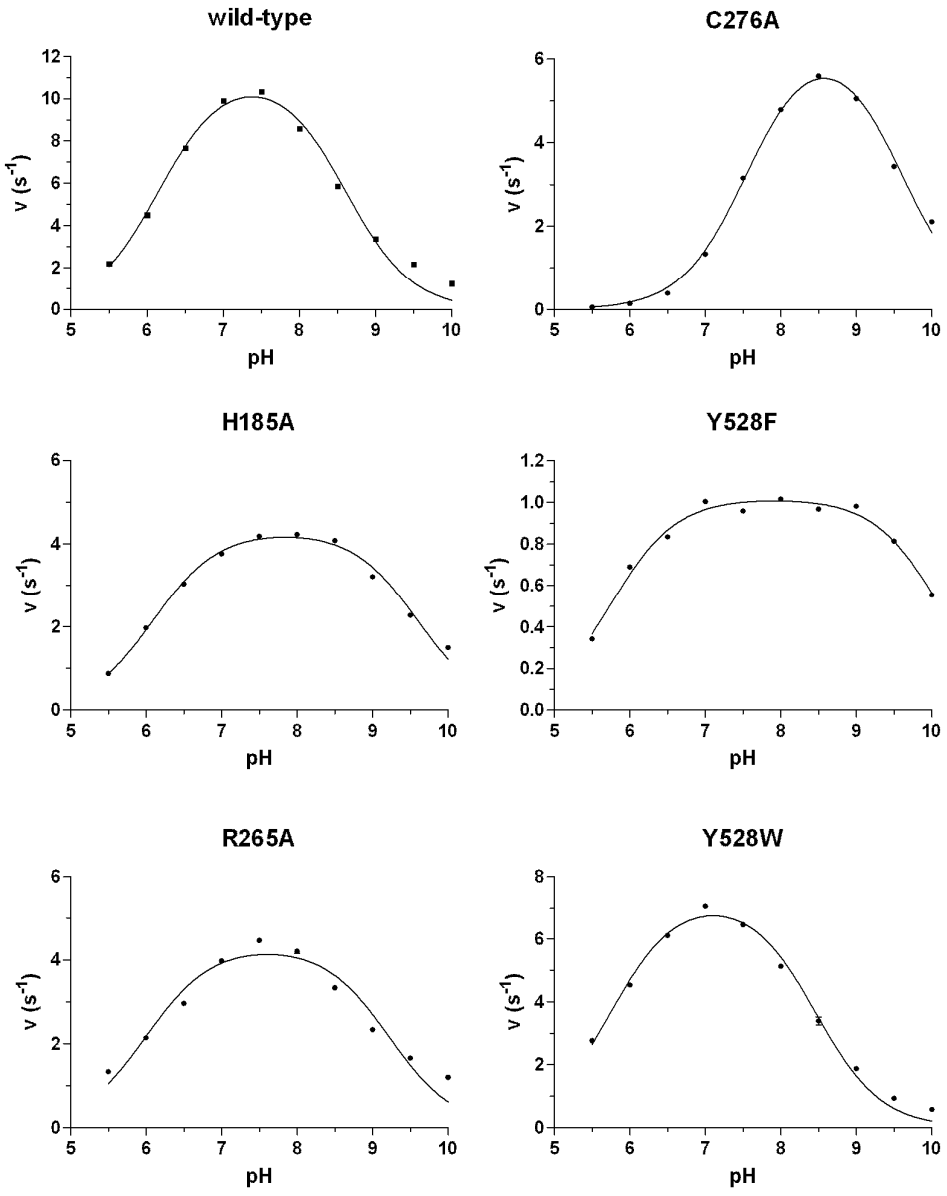

Figure 4-4 pH-dependent CoQ_D activity of wild-type and mutant *Pf* DHODH.

CHAPTER FIVE
Significance and Future Prospects

SIGNIFICANCE

The research presented here sheds new light onto the oxidative half-reaction of *Pf* DHODH. The means by which the enzyme interacts with ubiquinone substrates is identified and a model of how electrons are transmitted to those substrates is proposed. The results answer several unresolved questions regarding the Family 2 DHODH catalytic mechanism and mode of inhibition.

Prior these studies, no ubiquinone-utilizing enzyme had been analyzed using the surface dilution kinetics regime. Adopting that system first required the demonstration that these substrates were indeed present in detergent micelles. This was accomplished by adapting methods which were originally developed to examine detergent molecules partitioning into membranes. Indeed, this is also the first thermodynamic examination by isothermal titration calorimetry of ubiquinone analogues partitioning into detergent micelles. The results define the integral role of detergents in catalysis, a role that had previously been rationalized as important for either enzyme or substrate solubility, but not necessarily important for the interaction between the enzyme and substrate.

The reductive half-reactions of several DHODH enzymes have been studied using steady-state and pre-steady-state kinetics in conjunction with mutagenesis and heavy-atom-labeled substrates. However, this body of work is

the first extensive mutagenesis study of the oxidative half-reaction of any DHODH enzyme, and it is the first to use mutagenesis in combination with pre-steady-state kinetics to analyze this reaction. Though no DHODH enzyme has been co-crystallized with a ubiquinone substrate, steady-state kinetic data has indicated that the ubiquinone binding site is at least partially shared with inhibitors that have been co-crystallized with Family 2 enzymes. The work presented here reveals that inhibitors specifically block electron transfer to ubiquinone substrates, finally offering direct proof that the ubiquinone co-substrate binding site is in fact in the vicinity of these inhibitors. However, the rapid kinetic analysis of the CoQ_1-dependent oxidative half-reaction show mutations which significantly alter inhibitor binding to this site do not display a significant effect on the K_d for CoQ_1. The electron transfer model I have developed explains how inhibitors can block the oxidative half-reaction without necessitating an overlapping binding site with ubiquinone substrates.

The combined results explain the lack of any K_M^{app} effect on ubiquinone analogue catalysis upon mutation to alanine of numerous residues within van der Waals contact with A77 1726. The original hypothesis was that the A77 1726 binding site is (at least partially) the ubiquinone binding site. No steady-state data ever unambiguously confirmed this assumption. This situation of not being able to define the ubiquinone site by kinetic approaches prompted the ultimately unsuccessful search for a ubiquinone binding assay. However, if ubiquinone

substrates are presented on the surface of detergent micelles, and electrons are transmitted from FMN through residues in the A77 1726 site to a distant co-substrate binding site, then mutation of those residues would only produce a k_{cat} effect, and only for residues involved in the electron transfer pathway. The data from this body of work support such a parsimonious model.

FUTURE PROSPECTS

Interfacial Kinetics

The interfacial kinetics experiments were performed near the limits of that system due to the finite solubility of ubiquinone analogues. Long-chained ubiquinone analogues were found to partition into detergent micelles to a significant extent, but, as one reviewer noted, this leads to a finite quantity of co-substrate free in solution directly proportional to the amount of total co-substrate. The applicability of the system was proven by calculating the amount of co-substrate free in solution. Under the conditions used, only sub-micromolar concentrations of co-substrate are present in solution, and these concentrations change very little for conditions which define a particular kinetic curve.

It may be possible to perform interfacial kinetic experiments using liposomes and ubiquinone co-substrates containing eight or nine isoprene unit tails. This would produce a more physiologically relevant environment in which to assess the effect of mutation on catalysis or to test inhibitors. The background

absorbance produced by the presence of liposomes would necessitate the development of a different spectroscopic kinetic assay or a new assay altogether.

Rapid Kinetics

Similar to the interfacial kinetic analysis of *Pf* DHODH, the rapid kinetic analysis of the CoQ-dependent reaction were performed near the limit of the available instrumentation. The most informative experiments regarding both the reductive and oxidative DHODH half-reactions would involve multi-wavelength studies, ideally under strictly anaerobic conditions. Multi-wavelength analysis allows the entire FMN spectrum to be observed during the course of an enzymatic reaction. The extra information contained within the FMN spectra can reveal processes such as formation of a DHO-enzyme charge-transfer complex, presence of a semiquinone intermediate, and dissociation of the product orotate. Additionally, spectra can be globally fitted to produce a kinetic model which accounts for reaction intermediates.

The rapid kinetics experiments observing the *Pf* DHODH oxidative half-reaction described in this work were done under anaerobic conditions using the glucose oxidase and catalase system by reducing enzyme with a sub-stochiometric amount of DHO, then mixing reduced enzyme with excess CoQ_1 and observing FMN re-oxidation. These experiments necessarily contained the product orotic acid, which may have an effect on the oxidative half-reaction. Enzyme reduction by titrating with an inorganic reductant such as dithionite, under strictly anaerobic

conditions, would allow the determination of the effect of orotic acid on the oxidative half-reaction.

Strictly anaerobic multi-wavelength stopped-flow experiments would greatly minimize any background problems and would allow additional information to be collected for both DHODH half-reactions. Any future rapid kinetic analysis of *Pf* DHODH would be best performed under strictly anaerobic conditions and take advantage of multi-wavelength analysis if at all possible.

Additional Mutagenesis

In addition to the *Pf* DHODH residues within 4 Å of the inhibitor A77 1726 chosen for mutagenesis in Chapter Three, several other residues were examined by steady-state kinetics but found not to alter any kinetic parameters to a significant extent. Certainly, this does not ensure that every residue involved in the oxidative half-reaction of *Pf* DHODH has been identified, and candidate residues still remain. Residues near I272 with side-chains that could transmit electrons from that residue to a distant CoQ binding site could be investigated. Also, residues further out from FMN, likely "facing outward" from the N-terminal helical domain could be involved in CoQ binding and/or catalysis.

Another line of investigation could involve the two other well-studied Family 2 DHODH enzymes from *E. coli* and human. These studies would begin with a kinetic analysis of the conserved or semi-conserved residues found in the *Plasmodium* enzyme to be involved in electron transfer to CoQ substrates.

Identification of residues as important for catalysis in other Family 2 DHODH enzymes would further support the hypothesis that electrons travel through residue side-chains to a distant CoQ substrates binding site.

BIBLIOGRAPHY

1. Miller, L.H., et al., *The pathogenic basis of malaria.* Nature, 2002. **415**(6872): p. 673-9.
2. Breman, J.G., M.S. Alilio, and A. Mills, *Conquering the intolerable burden of malaria: what's new, what's needed: a summary.* Am J Trop Med Hyg, 2004. **71**(2 Suppl): p. 1-15.
3. Foth, B.J. and G.I. McFadden, *The apicoplast: a plastid in Plasmodium falciparum and other Apicomplexan parasites.* Int Rev Cytol, 2003. **224**: p. 57-110.
4. Ralph, S.A., M.C. D'Ombrain, and G.I. McFadden, *The apicoplast as an antimalarial drug target.* Drug Resist Updat, 2001. **4**(3): p. 145-51.
5. Hyde, J.E., *Drug-resistant malaria.* Trends Parasitol, 2005. **21**(11): p. 494-8.
6. Ridley, R.G., *Medical need, scientific opportunity and the drive for antimalarial drugs.* Nature, 2002. **415**(6872): p. 686-93.
7. Rosenthal, P.J., *Antimalarial chemotherapy : mechanisms of action, resistance, and new directions in drug discovery*. 2001, Totowa, N.Y.: Humana Press. xi, 396 p.
8. Duraisingh, M.T., et al., *Increased sensitivity to the antimalarials mefloquine and artemisinin is conferred by mutations in the pfmdr1 gene of Plasmodium falciparum.* Mol Microbiol, 2000. **36**(4): p. 955-61.
9. Fidock, D.A., et al., *Mutations in the P. falciparum digestive vacuole transmembrane protein PfCRT and evidence for their role in chloroquine resistance.* Mol Cell, 2000. **6**(4): p. 861-71.
10. Eckstein-Ludwig, U., et al., *Artemisinins target the SERCA of Plasmodium falciparum.* Nature, 2003. **424**(6951): p. 957-61.
11. Korsinczky, M., et al., *Mutations in Plasmodium falciparum cytochrome b that are associated with atovaquone resistance are located at a putative drug-binding site.* Antimicrob Agents Chemother, 2000. **44**(8): p. 2100-8.
12. Choi, S.R., et al., *Design, Synthesis, and Biological Evaluation of Plasmodium falciparum Lactate Dehydrogenase Inhibitors.* J Med Chem, 2007. **50**(16): p. 3841-50.
13. Sherman, I.W., *Transport of amino acids and nucleic acid precursors in malarial parasites.* Bull World Health Organ, 1977. **55**(2-3): p. 211-25.
14. Kuo, M.R., et al., *Targeting tuberculosis and malaria through inhibition of Enoyl reductase: compound activity and structural data.* J Biol Chem, 2003. **278**(23): p. 20851-9.
15. Wiesner, J. and H. Jomaa, *Isoprenoid biosynthesis of the apicoplast as drug target.* Curr Drug Targets, 2007. **8**(1): p. 3-13.

16. Gero, A.M. and W.J. O'Sullivan, *Purines and pyrimidines in malarial parasites.* Blood Cells, 1990. **16**(2-3): p. 467-84; discussion 485-98.
17. Nara, T., T. Hshimoto, and T. Aoki, *Evolutionary implications of the mosaic pyrimidine-biosynthetic pathway in eukaryotes.* Gene, 2000. **257**(2): p. 209-22.
18. Norager, S., et al., *E-coli dihydroorotate dehydrogenase reveals structural and functional distinctions between different classes of dihydroorotate dehydrogenases.* Structure, 2002. **10**(9): p. 1211-1223.
19. Rawls, J., et al., *Requirements for the mitochondrial import and localization of dihydroorotate dehydrogenase.* Eur J Biochem, 2000. **267**(7): p. 2079-87.
20. Nagy, M., F. Lacroute, and D. Thomas, *Divergent evolution of pyrimidine biosynthesis between anaerobic and aerobic yeasts.* Proc Natl Acad Sci U S A, 1992. **89**(19): p. 8966-70.
21. Jones, M.E., *Pyrimidine nucleotide biosynthesis in animals: genes, enzymes, and regulation of UMP biosynthesis.* Annu Rev Biochem, 1980. **49**: p. 253-79.
22. Andersen, P.S., P.J. Jansen, and K. Hammer, *Two different dihydroorotate dehydrogenases in Lactococcus lactis.* J Bacteriol, 1994. **176**(13): p. 3975-82.
23. Krungkrai, J., *Purification, characterization and localization of mitochondrial dihydroorotate dehydrogenase in Plasmodium falciparum, human malaria parasite.* Biochim Biophys Acta, 1995. **1243**(3): p. 351-60.
24. Krungkrai, J., A. Cerami, and G.B. Henderson, *Purification and characterization of dihydroorotate dehydrogenase from the rodent malaria parasite Plasmodium berghei.* Biochemistry, 1991. **30**(7): p. 1934-9.
25. de Macedo, C.S., et al., *Characterization of the isoprenoid chain of coenzyme Q in Plasmodium falciparum.* FEMS Microbiol Lett, 2002. **207**(1): p. 13-20.
26. Baldwin, J., et al., *Malarial dihydroorotate dehydrogenase. Substrate and inhibitor specificity.* J Biol Chem, 2002. **277**(44): p. 41827-34.
27. Liu, S., et al., *Structures of human dihydroorotate dehydrogenase in complex with antiproliferative agents.* Structure Fold Des, 2000. **8**(1): p. 25-33.
28. Copeland, R.A., et al., *Recombinant human dihydroorotate dehydrogenase: expression, purification, and characterization of a catalytically functional truncated enzyme.* Arch Biochem Biophys, 1995. **323**(1): p. 79-86.

29. Ullrich, A., et al., *Recombinant expression of N-terminal truncated mutants of the membrane bound mouse, rat and human flavoenzyme dihydroorotate dehydrogenase. A versatile tool to rate inhibitor effects?* Eur J Biochem, 2001. **268**(6): p. 1861-8.
30. Davis, J.P., et al., *The immunosuppressive metabolite of leflunomide is a potent inhibitor of human dihydroorotate dehydrogenase.* Biochemistry, 1996. **35**(4): p. 1270-3.
31. Rowland, P., et al., *The crystal structure of the flavin containing enzyme dihydroorotate dehydrogenase A from Lactococcus lactis.* Structure, 1997. **5**(2): p. 239-252.
32. Rowland, P., et al., *Structure of dihydroorotate dehydrogenase B: Electron transfer between two flavin groups bridged by an iron-sulphur cluster.* Structure, 2000. **8**(12): p. 1227-1238.
33. Hansen, M., et al., *Inhibitor binding in a class 2 dihydroorotate dehydrogenase causes variations in the membrane-associated N-terminal domain.* Protein Science, 2004. **13**(4): p. 1031-1042.
34. Hurt, D.E., J. Widom, and J. Clardy, *Structure of Plasmodium falciparum dihydroorotate dehydrogenase with a bound inhibitor.* Acta Crystallogr D Biol Crystallogr, 2006. **62**(Pt 3): p. 312-23.
35. Baldwin, J., et al., *High-throughput screening for potent and selective inhibitors of Plasmodium falciparum dihydroorotate dehydrogenase.* J Biol Chem, 2005. **280**(23): p. 21847-53.
36. Bjornberg, O., et al., *The activity of Escherichia coli dihydroorotate dehydrogenase is dependent on a conserved loop identified by sequence homology, mutagenesis, and limited proteolysis.* Biochemistry, 1999. **38**(10): p. 2899-908.
37. Bjornberg, O., et al., *Active site of dihydroorotate dehydrogenase A from Lactococcus lactis investigated by chemical modification and mutagenesis.* Biochemistry, 1997. **36**(51): p. 16197-205.
38. Fagan, R.L., et al., *Mechanism of Flavin Reduction in the Class 1A Dihydroorotate Dehydrogenase from Lactococcus lactis.* Biochemistry, 2007. **46**(13): p. 4028-36.
39. Argyrou, A., M.W. Washabaugh, and C.M. Pickart, *Dihydroorotate dehydrogenase from Clostridium oroticum is a class 1B enzyme and utilizes a concerted mechanism of catalysis.* Biochemistry, 2000. **39**(34): p. 10373-84.
40. Pascal, R.A., Jr. and C.T. Walsh, *Mechanistic studies with deuterated dihydroorotates on the dihydroorotate oxidase from Crithidia fasciculata.* Biochemistry, 1984. **23**(12): p. 2745-52.
41. Fagan, R.L., et al., *Mechanism of flavin reduction in class 2 dihydroorotate dehydrogenases.* Biochemistry, 2006. **45**(50): p. 14926-32.

42. Palfey, B.A., O. Bjornberg, and K.F. Jensen, *Insight into the chemistry of flavin reduction and oxidation in Escherichia coli dihydroorotate dehydrogenase obtained by rapid reaction studies.* Biochemistry, 2001. **40**(14): p. 4381-90.
43. Hines, V. and M. Johnston, *Analysis of the kinetic mechanism of the bovine liver mitochondrial dihydroorotate dehydrogenase.* Biochemistry, 1989. **28**(3): p. 1222-6.
44. Bjornberg, O., et al., *Dihydrooxonate is a substrate of dihydroorotate dehydrogenase (DHOD) providing evidence for involvement of cysteine and serine residues in base catalysis.* Arch Biochem Biophys, 2001. **391**(2): p. 286-94.
45. Hines, V. and M. Johnston, *Mechanistic studies on the bovine liver mitochondrial dihydroorotate dehydrogenase using kinetic deuterium isotope effects.* Biochemistry, 1989. **28**(3): p. 1227-34.
46. Davis, J.P. and R.A. Copeland, *Histidine to alanine mutants of human dihydroorotate dehydrogenase. Identification of a brequinar-resistant mutant enzyme.* Biochem Pharmacol, 1997. **54**(4): p. 459-65.
47. Palfey, B.A., O. Bjornberg, and K.F. Jensen, *Specific inhibition of a family 1A dihydroorotate dehydrogenase by benzoate pyrimidine analogues.* J Med Chem, 2001. **44**(18): p. 2861-4.
48. Knecht, W. and M. Loffler, *Redoxal as a new lead structure for dihydroorotate dehydrogenase inhibitors: a kinetic study of the inhibition mechanism.* FEBS Lett, 2000. **467**(1): p. 27-30.
49. Greene, S., et al., *Inhibition of dihydroorotate dehydrogenase by the immunosuppressive agent leflunomide.* Biochem Pharmacol, 1995. **50**(6): p. 861-7.
50. Knecht, W. and M. Loffler, *Species-related inhibition of human and rat dihydroorotate dehydrogenase by immunosuppressive isoxazol and cinchoninic acid derivatives.* Biochem Pharmacol, 1998. **56**(9): p. 1259-64.
51. McLean, J.E., et al., *Multiple inhibitor analysis of the brequinar and leflunomide binding sites on human dihydroorotate dehydrogenase.* Biochemistry, 2001. **40**(7): p. 2194-200.
52. Carman, G.M., R.A. Deems, and E.A. Dennis, *Lipid signaling enzymes and surface dilution kinetics.* J Biol Chem, 1995. **270**(32): p. 18711-4.
53. Jain, M.K. and O.G. Berg, *The kinetics of interfacial catalysis by phospholipase A2 and regulation of interfacial activation: hopping versus scooting.* Biochim Biophys Acta, 1989. **1002**(2): p. 127-56.
54. Gelb, M.H., J.H. Min, and M.K. Jain, *Do membrane-bound enzymes access their substrates from the membrane or aqueous phase: interfacial*

versus non-interfacial enzymes. Biochim Biophys Acta, 2000. **1488**(1-2): p. 20-7.

55. Deems, R.A., B.R. Eaton, and E.A. Dennis, *Kinetic analysis of phospholipase A2 activity toward mixed micelles and its implications for the study of lipolytic enzymes.* J Biol Chem, 1975. **250**(23): p. 9013-20.
56. Deems, R.A., *Interfacial enzyme kinetics at the phospholipid/water interface: practical considerations.* Anal Biochem, 2000. **287**(1): p. 1-16.
57. Engel, W.D., H. Schagger, and G. von Jagow, *Ubiquinol-cytochrome c reductase (EC 1.10.2.2). Isolation in triton X-100 by hydroxyapatite and gel chromatography. Structural and functional properties.* Biochim Biophys Acta, 1980. **592**(2): p. 211-22.
58. Chattopadhyay, A. and E. London, *Fluorimetric determination of critical micelle concentration avoiding interference from detergent charge.* Anal Biochem, 1984. **139**(2): p. 408-12.
59. Karibian, D., *Dihydroorotate dehydrogenase (Escherichia coli).* Methods Enzymol, 1978. **51**: p. 58-63.
60. Seelig, J. and P. Ganz, *Nonclassical hydrophobic effect in membrane binding equilibria.* Biochemistry, 1991. **30**(38): p. 9354-9.
61. Heerklotz, H. and J. Seelig, *Titration calorimetry of surfactant-membrane partitioning and membrane solubilization.* Biochim Biophys Acta, 2000. **1508**(1-2): p. 69-85.
62. Heerklotz, H., et al., *Thermodynamic characterization of dilute aqueous lipid/detergent mixtures of POPC and C(12)EO(8) by means of isothermal titration calorimetry.* Journal of Physical Chemistry, 1996. **100**(16): p. 6764-6774.
63. Heerklotz, H. and J. Seelig, *Correlation of membrane/water partition coefficients of detergents with the critical micelle concentration.* Biophys J, 2000. **78**(5): p. 2435-40.
64. Vial, H.J., et al., *Phospholipids in parasitic protozoa.* Mol Biochem Parasitol, 2003. **126**(2): p. 143-54.
65. Buxeda, R.J., et al., *Phosphatidylinositol 4-kinase from Saccharomyces cerevisiae. Kinetic analysis using Triton X-100/phosphatidylinositol-mixed micelles.* J Biol Chem, 1991. **266**(21): p. 13859-65.
66. Qin, C., C. Wang, and X. Wang, *Kinetic analysis of Arabidopsis phospholipase Ddelta. Substrate preference and mechanism of activation by Ca2+ and phosphatidylinositol 4,5-biphosphate.* J Biol Chem, 2002. **277**(51): p. 49685-90.
67. Carman, G.M. and W. Dowhan, *Phosphatidylserine synthase from Escherichia coli. The role of Triton X-100 in catalysis.* J Biol Chem, 1979. **254**(17): p. 8391-7.

68. Nickels, J.T., Jr., R.J. Buxeda, and G.M. Carman, *Purification, characterization, and kinetic analysis of a 55-kDa form of phosphatidylinositol 4-kinase from Saccharomyces cerevisiae.* J Biol Chem, 1992. **267**(23): p. 16297-304.
69. Han, G.S., W.I. Wu, and G.M. Carman, *The Saccharomyces cerevisiae Lipin homolog is a Mg2+-dependent phosphatidate phosphatase enzyme.* J Biol Chem, 2006. **281**(14): p. 9210-8.
70. Wu, W.I., et al., *Purification and characterization of diacylglycerol pyrophosphate phosphatase from Saccharomyces cerevisiae.* J Biol Chem, 1996. **271**(4): p. 1868-76.
71. Wu, W.I. and G.M. Carman, *Regulation of phosphatidate phosphatase activity from the yeast Saccharomyces cerevisiae by nucleotides.* J Biol Chem, 1994. **269**(47): p. 29495-501.
72. Wu, W.I. and G.M. Carman, *Regulation of phosphatidate phosphatase activity from the yeast Saccharomyces cerevisiae by phospholipids.* Biochemistry, 1996. **35**(12): p. 3790-6.
73. Wu, W.I., et al., *Regulation of phosphatidate phosphatase activity from the yeast Saccharomyces cerevisiae by sphingoid bases.* J Biol Chem, 1993. **268**(19): p. 13830-7.
74. Hurt, D.E., A.E. Sutton, and J. Clardy, *Brequinar derivatives and species-specific drug design for dihydroorotate dehydrogenase.* Bioorg Med Chem Lett, 2006. **16**(6): p. 1610-5.
75. Heikkila, T., et al., *The first de novo designed inhibitors of Plasmodium falciparum dihydroorotate dehydrogenase.* Bioorg Med Chem Lett, 2006. **16**(1): p. 88-92.
76. Boa, A.N., et al., *Synthesis of brequinar analogue inhibitors of malaria parasite dihydroorotate dehydrogenase.* Bioorg Med Chem, 2005. **13**(6): p. 1945-67.
77. Combe, J.P., et al., *Lys-D48 is required for charge stabilization, rapid flavin reduction, and internal electron transfer in the catalytic cycle of dihydroorotate dehydrogenase B of Lactococcus lactis.* J Biol Chem, 2006. **281**(26): p. 17977-88.
78. Malmquist, N.A., J. Baldwin, and M.A. Phillips, *Detergent-dependent kinetics of truncated Plasmodium falciparum dihydroorotate dehydrogenase.* J Biol Chem, 2007. **282**(17): p. 12678-86.
79. Shi, J., et al., *Multiple states of the Tyr318Leu mutant of dihydroorotate dehydrogenase revealed by single-molecule kinetics.* J Am Chem Soc, 2004. **126**(22): p. 6914-22.
80. Gray, H.B. and J.R. Winkler, *Electron tunneling through proteins.* Q Rev Biophys, 2003. **36**(3): p. 341-72.

81. Moser, C.C., C.C. Page, and P.L. Dutton, *Darwin at the molecular scale: selection and variance in electron tunnelling proteins including cytochrome c oxidase.* Philos Trans R Soc Lond B Biol Sci, 2006. **361**(1472): p. 1295-305.
82. Sutcliffe, M.J., et al., *Hydrogen tunnelling in enzyme-catalysed H-transfer reactions: flavoprotein and quinoprotein systems.* Philos Trans R Soc Lond B Biol Sci, 2006. **361**(1472): p. 1375-86.
83. Newman, J., *Novel buffer systems for macromolecular crystallization.* Acta Crystallogr D Biol Crystallogr, 2004. **60**(Pt 3): p. 610-2.
84. Marcinkeviciene, J., et al., *A second dihydroorotate dehydrogenase (Type A) of the human pathogen Enterococcus faecalis: expression, purification, and steady-state kinetic mechanism.* Arch Biochem Biophys, 2000. **377**(1): p. 178-86.
85. Marcinkeviciene, J., et al., *Dihydroorotate dehydrogenase B of Enterococcus faecalis. Characterization and insights into chemical mechanism.* Biochemistry, 1999. **38**(40): p. 13129-37.

VITAE

Nicholas Anthony Malmquist was born in Reno, Nevada, on March 6, 1978, the son of Nancie Jean Malmquist and Dr. Kenneth Wesley Malmquist, M.D. (a graduate of UT Southwestern Medical School). After graduating from Sparks High School in his hometown of Sparks, Nevada, he went to Whitman College in Walla Walla, Washington. He spent two summers back home at the University of Nevada Medical School in Reno, Nevada and one summer at Oregon State University in Corvallis, Oregon working on various research projects. He received his Bachelor of Arts degree from Whitman College in a combined Biology-Chemistry program with a minor in Astronomy in May, 2000. The following year he worked as a laboratory technician for Dr. Iain Buxton at the University of Nevada Medical School. He enrolled at the University of Texas Southwestern Medical Center at Dallas in the fall of 2001 and joined the laboratory of Dr. Margaret Phillips in the spring of 2002. After encouragement from Dr. Phillips, he participated in the Biology of Parasitism course at the Marine Biological Laboratory in Woods Hole, MA in the summer of 2003 as a student and again as a teaching assistant in the summer of 2006. He married his college girlfriend, Camille Rebekka Keedy, in the spring of 2006. After graduating with a Ph.D. in the Biological Chemistry program in the fall of 2007 he is accepting a post-doctoral position at the Pasteur Institute in Paris, France.

Permanent Address: 5705 Wedekind Road
Sparks, Nevada, 89431